Journal of Marine Research, 72, 405–444, 2014

Diatom control of the autotrophic community and particle export in the eastern Bering Sea during the recent cold years (2008–2010)

by Matthew S. Baumann[1,2,3], S. Bradley Moran[1], Michael W. Lomas[4], Roger P. Kelly[1], Douglas W. Bell[5], and Jeffrey W. Krause[6]

ABSTRACT

The southeastern Bering Sea has exhibited shifts in climate since the start of the 21st century. The regional climate shifts are manifested in the duration and areal extent of seasonal sea-ice coverage. During a recent cold period (2008–2010) with extensive spring sea-ice cover over the southeastern shelf of the Bering Sea, a total of 77 water column and 24 sediment trap profiles were collected over the shelf and shelf break and analyzed for autotrophic pigment concentrations and elemental (carbon, nitrogen, phosphorus, and silicon) concentrations in suspended and exported particulate material. These results are used to establish the seasonal succession of the autotrophic community and the control that both phytoplankton and zooplankton exert on export production. In spring (April to mid-June), total chlorophyll *a* (TChl *a*) concentrations were generally low (i.e., <1 $\mu g\ L^{-1}$); however, localized phytoplankton blooms near the marginal ice zone (MIZ) lead to elevated spring average TChl *a* concentrations (i.e., >5 $\mu g\ L^{-1}$). In summer (mid-June to late July), photic zone chlorophyll *a* concentrations were typically <1 $\mu g\ L^{-1}$ over the shelf and at the shelf break. Diatoms represented the greatest contribution to TChl *a* (regional averages of 71%–96% in spring and 25%–75% in summer) and autotrophic biomass in spring and summer. This algal class also represented 50%–99% of TChl *a* associated with particles sinking from the photic zone. The relatively high proportion of phaeophorbide *a* in sediment trap material indicates that sinking of zooplankton fecal pellets facilitate the export of particles through the water column. Further, zooplankton grazing may be an important process that returns regenerated nutrients to the water column based on the elemental composition of suspended and sinking particles. In colder than average years, the emergence of diatom blooms in the spring MIZ supports the production of abundant large zooplankton, which are a primary food source for juvenile pelagic fishes of economically important species. Therefore,

1. Graduate School of Oceanography, University of Rhode Island, Narragansett, RI 02882-1197
2. Present address: Industrial Economics Inc., Cambridge, MA 02140
3. Corresponding author: ***e-mail: matthew_baumann@my.uri.edu***
4. Bigelow Laboratory for Ocean Sciences, East Boothbay, ME 04544
5. Marine Science Program, University of South Carolina, Columbia, SC 29205
6. Dauphin Island Sea Lab, Dauphin Island, AL 36528

processes in colder than average years may be essential for the transfer of particulate organic carbon from the surface waters and the success of the economically important pelagic fisheries.

Keywords. Bering Sea, phytoplankton, particle export, particulate organic carbon, diatom, biogenic silica

1. Introduction

The eastern Bering Sea supports some of the highest seasonal rates of primary production in the world ocean (Springer et al. 1996). Such high levels of primary production over the broad (~500 km wide) and vast (~10,000 km^2) shelf support one of the largest fisheries in the United States in terms of fish catch revenue and landings according to National Marine Fisheries Service data. The seasonal extent and duration of sea ice represents the most important constraint on the location, timing, and magnitude of spring primary production (Alexander and Niebauer 1981; Stabeno et al. 2010) and the composition of the autotrophic community (Schandelmeier and Alexander 1981). The lowest trophic levels of the ecosystem exhibit marked variability in distribution and abundance in response to changes in sea ice in this region (e.g., Napp and Hunt 2001; Stabeno, Farley, et al. 2012; Stabeno, Kachel, et al. 2012). Because the physical regime exerts a strong control on the spring bloom and carbon flow through phytoplankton and zooplankton (Lovvorn et al. 2005), changes in seasonal sea-ice extent and duration are predicted to impact the distribution and abundance of higher trophic level and economically important organisms in both the southeastern and northern regions of the shelf (Hunt et al. 2002; Grebmeier, Overland, et al. 2006; Cooper et al. 2013).

In colder than average years, maximum sea-ice extent reaches the shelf break of the southeastern Bering Sea (Stabeno, Kachel, et al. 2012). Spring phytoplankton production is often dominated by intense diatom blooms as sea ice retreats over nutrient rich water along the shelf break (Schandelmeier and Alexander 1981). The diatom blooms are initiated by increasing stability of the upper water column that is induced by stratification from meltwater released from the retreating ice edge. This region is commonly referred to as the marginal ice zone (MIZ) (Alexander and Niebauer 1981; Schandelmeier and Alexander 1981). More than half of the annual primary production occurs between May and July in this region, a seasonal pulse that is controlled by the presence of sea ice (Brown, van Dijken, and Arrigo 2011). Ice-edge blooms are terminated by nutrient limitation (Niebauer, Alexander, and Henrichs 1995). The post–ice-edge bloom phytoplankton community is still largely composed of diatoms; however, other algal groups, such as flagellates and haptophytes (namely *Phaeocystis pouchetti*), emerge as important autotrophic contributors (Suzuki et al. 2002; Fujiki et al. 2009; Lomas et al. 2012; Moran et al. 2012). The relationship between the magnitude and composition of newly formed organic carbon and of particles exported from the photic zone bears on carbon linkages between lower trophic levels and of pelagic and benthic ecosystems.

The midspring development of the MIZ bloom in cold years, perhaps in conjunction with under ice and ice-algae primary production (Horner and Schrader 1982; Syvertsen

1991), largely supports the production of abundant larger copepods and euphausiids such as *Calanus marshallae* and *Thysanoessa raschii*, which are less prevalent during warm years (Hunt et al. 2011). Large zooplankton constitute a lipid-rich prey source for young age classes of walleye pollock (*Theragra chalcogramma*), and the presence of these secondary producers is necessary for the success of the age-0 year class (Hunt et al. 2011; Heintz et al. 2013; Siddon, Heintz, and Meuter 2013) and other pelagic consumers. Primary production may be exported to deeper waters or to the benthos as particulate organic carbon (POC) by the sinking of intact algal cells (Grebmeier, Cooper, et al. 2006; Cooper et al. 2012). The sinking flux of zooplankton fecal pellets also represents an important pathway for the transfer of POC from the surface waters to the benthos of high-latitude shelf systems (Juul-Pedersen et al. 2006; Wassmann et al. 2006; Juul-Pedersen, Michel, and Gosselin 2010; Gleiber, Steinberg, and Ducklow 2012). Therefore, in cold years, abundant large zooplankton not only support young age classes of economically important animals, but also exert an important control on the export flux of POC from the upper water column.

This study investigates the seasonal succession of the autotrophic community and the controls that both phytoplankton and zooplankton have on the export of particulate organic matter (POM) from the photic zone during a 3-year segment (2008–2010) of a recent cold period in the eastern Bering Sea. The specific objectives of this study are to determine (1) the seasonal evolution of the autotrophic community over the shelf and shelf break using total chlorophyll *a* (TChl *a*) and algal class–specific indicator pigments ratios and (2) the influence that zooplankton exert on export using degraded chlorophyll *a* (total phaeopigments [Σphaeopigments]) and C:N:P ratios of sinking particles. The results of this study indicate that both primary production and particle flux are dominated by diatoms, and, during such cold years, the sinking of fecal pellets from large zooplankton represents an important component of the particle export flux.

2. Methods

Sediment trap and water column samples were collected in the eastern Bering Sea during spring and summer cruises from 2008 to 2010 as part of the Bering Ecosystem Study–Bering Sea Integrated Ecosystem Research Project field program (Table 1). For the purpose of this study, the regions of the U.S. Bering Sea Exclusive Economic Zone (marine regions of the Bering Sea; http://bsierp.nprb.org/) are grouped into seven geographically larger regions (Fig. 1). Additionally, data were further binned into spring (cruises HLY0802, HLY0902, and TN249) and summer (cruises HLY0803, KN195-10, and TN250) seasons. Coordinates for individual stations are listed in Table A1.

Hydrographic measurements were collected during each cast of the CTD (conductivity, temperature, depth) rosette. The CTD profiler was an SBE (Sea-bird Electronics, Bellevue, WA) 911+, equipped with an SBE-3 temperature sensor, an SBE-4 conductivity sensor, an SBE-43 dissolved oxygen (DO) sensor, a Chelsea Aquatrack3 fluorometer, and a Biospherical QSP2300 photosynthetically active radiation sensor. The sensors were calibrated prior to each field year. This rosette was outfitted with acid-cleaned 30 L Niskin bottles used for water sample collection.

Table 1. List of cruises and number of sampling profiles collected during the 2008–2010 NSF North Pacific Research Board Bering Ecosystem Study–Bering Sea Integrated Ecosystem Research Project field program.

Cruise	Season	Vessel	Dates	No. water column samples	No. traps
HLY0802	Spring 2008	USCGC *Healy*	29 March–6 May 2008	10	3
HLY0803	Summer 2008	USCGC *Healy*	3 July–31 July 2008	–	3
HLY0902	Spring 2009	USCGC *Healy*	31 March–12 May 2009	18	5
KN195-10	Summer 2009	R/V *Knorr*	14 June–13 July 2009	18	4
TN249	Spring 2010	R/V *T. G. Thompson*	9 May–14 June 2010	18	5
TN250	Summer 2010	R/V *T. G. Thompson*	16 June–13 July 2010	13	4

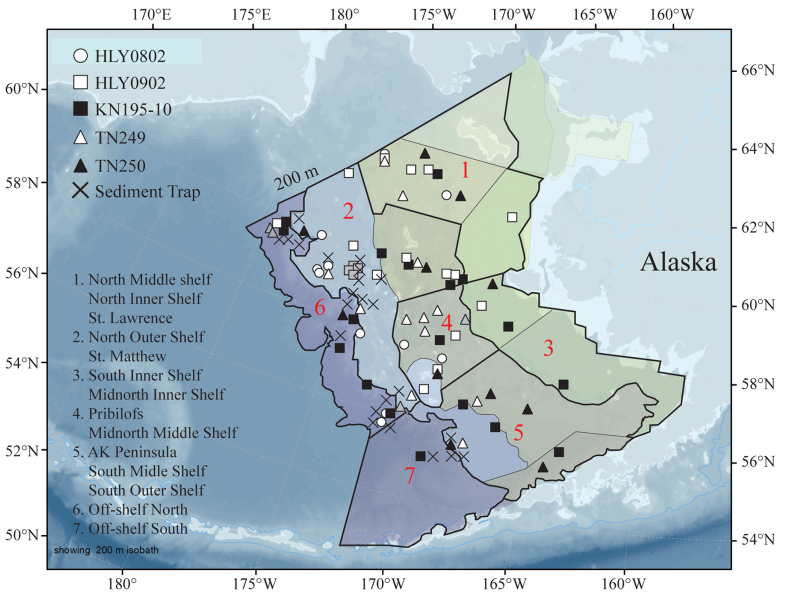

Figure 1. Map of the eastern Bering Sea study area. Thin lines delineate the regions designated during the Bering Ecosystem Study–Bering Sea Integrated Ecosystem Research Project (BEST-BSIERP) program. Bold lines represent the seven larger geographic regions used for data interpretation in this study. Listed on the figure are the BEST-BSIERP regions included in each larger geographic region. White (spring) and black (summer) symbols represent water column sampling locations during the field study (see Table 1 for cruise information). Cross symbols are sediment trap deployment locations. Gray symbols represent stations with total chlorophyll *a* concentrations exhibiting "bloom" conditions (i.e., $>5\ \mu g\ L^{-1}$).

a. Upper–water column particulate organic carbon, nitrogen, and phosphorus; biogenic silica; and autotrophic pigments

Concentrations of suspended POC, particulate organic nitrogen (PON), and particulate organic phosphorus (POP) in the water column were measured in 0.2 L samples collected from the CTD rosette. Samples were vacuum filtered onto precombusted (4 h at 450°C) 25 mm glass fiber filters (GF/F; 0.7 μm nominal pore size). Biogenic silica (bSi) concentrations were measured in 0.25 L samples and vacuum filtered onto 47 mm, 0.4 μm polycarbonate membrane filters. Total (>0.7 μm) water column pigments were measured in 1 L samples and vacuum filtered onto a 47 mm GF/F. All samples were frozen after filtration. POC, PON, POP, and bSi samples were frozen at −20°C, and pigment samples were stored at −80°C until analysis.

b. Sediment trap sampling

Sediment traps (KC Denmark, Silkeborg, Denmark) were deployed near the shelf break in water column depths >150 m (Fig. 1; n = 3 in spring and n = 3 in summer 2008; n = 5 in spring and n = 4 in summer 2009 and 2010). Trap tubes were filled with nonpoisoned, 0.4 μm filtered brine ($S = \sim 85\%$) prior to deployment to isolate swimmers and suspended particulates from passively sinking particles. Particle trap arrays (four trap tubes per depth; 72 mm mouth diameter × 450 mm tube length) were affixed to a surface-tethered, free-floating down line. Sediment traps collected sinking particles for ∼24 h at depths of 25, 40, 50, 60, and 100 m.

After recovery of the sediment trap arrays, the upper seawater layer was siphoned down to the seawater-brine interface, which was indicated by the discontinuity between the layers. Each trap tube was vacuum filtered onto a precombusted 25 mm GF/F. One full sediment trap tube per depth was used for HPLC pigment analysis, which was filtered and frozen at −80°C until analysis. Two additional tubes were used for POC and PON analysis. A stainless-steel arc punch was used to generate a 10 mm diameter subsample from each POC and PON GF/F, which were frozen at −20°C. For the 2010 cruises, a single trap tube was split into subsamples for POP and bSi analysis.

c. Analysis of POC, PON, POP, and bSi

Analysis of POC and PON followed the method described in Baumann, Moran, Lomas, et al. (2013). Briefly, the 10 mm subsamples from sediment trap GF/Fs were dried at 60°C in a drying oven, fumed with concentrated hydrochloric acid for 24 h to remove inorganic carbon, and dried again for 24 h at 60°C. POC and PON were measured using an EA-440 (Exeter Analytical Inc., North Chelmsford, MA) (Pike and Moran 1997). For each trap deployment, a field blank was prepared by filtering 200 mL of brine onto a GF/F. For each cruise, an average blank was subtracted from the gross POC and PON concentrations.

Sediment trap and water column POP samples were prepared using the ash-hydrolysis method, and orthophosphate concentrations were determined with the molybdate technique (Solórzano and Sharp 1980; Lomas et al. 2010, 2013).

The bSi samples were analyzed by sodium hydroxide (NaOH) digestion (Paasche 1973; Brzezinski and Nelson 1995). Teflon tubes were used for these analyses to achieve low and consistent blanks (Krause, Nelson, and Lomas 2009). The optical absorption of each sample was measured at 810 nm following the procedure of Strickland and Parsons (1968). Lithogenic silica (e.g., mineral dust, clays, and sands) was not measured. The fraction of lithogenic silica that dissolves during the NaOH digestion is small (<10%) and likely insignificant considering the high measured bSi concentrations.

d. Pigment analysis by HPLC

Autotrophic pigment analysis of sediment trap and water column samples was conducted at the University of Maryland Horn Point Laboratory by HPLC analysis (Van Heukelem and Thomas 2001). Samples were wrapped in foil and transported frozen in a liquid-nitrogen dry shipper to prevent pigment degradation. Briefly, samples were extracted using HPLC-grade (90%–100%) acetone and chilled while sonicated (model 450; Branson Ultrasonics, Danbury, CT). The extracts were clarified using a 0.45 μm Polytetrafluoroethylene (PTFE) HPLC syringe cartridge filter fitted with a GF/F prefilter (Scientific Resources Inc., Eatontown, NJ). Samples were analyzed using a Hewlett-Packard (Waldbronn, Germany) series 1100 HPLC equipped with a 900 μL syringe head autoinjector. Pigments were identified based on retention times of pure pigment standards or pigments isolated from algal monocultures.

e. Pigment analysis by CHEMTAX

The abundance of specific phytoplankton groups was estimated from indicator pigment concentrations relative to TChl *a* using the CHEMTAX program (Mackey et al. 1996). The initial matrix was adapted from two previous studies that determined relative phytoplankton abundances in the subarctic North Pacific (Suzuki et al. 2002; Fujiki et al. 2009). These studies determined pigment:TChl *a* ratios for the seed matrix by averaging minimum and maximum values listed in Mackey et al. (1996), except for diatoms in which they applied a fucoxanthin:TChl *a* (fuco:TChl *a*) ratio of 0.75 based on observations from a previous study (Obayashi et al. 2001). The same initial matrix was adopted in this study and used for all water column and sediment trap samples. This study focuses on three phytoplankton groups (diatoms, chlorophytes, and prymnesiophytes) as the pigments associated with these groups are present in greater concentrations relative to those associated with other phytoplankton classes. The CHEMTAX program provides relative abundances for five additional algal classes (pelagophytes, prasinophytes, cryptophytes, dinoflagellates, and cyanobacteria), and these values are also reported.

For most algal classes, the pigment:TChl *a* ratios selected for the initial matrix generally agree to within a factor of ∼2 with those calculated in the final matrix for both the water column and trap CHEMTAX analyses (Table A2). By comparison, the final matrix ratios for the water column and sediment trap data fall within the range of values reported by

Mackey et al. (1996) for the Southern Ocean. A sensitivity analysis was conducted using fuco:TChl *a* ratios of 0.35 and 1.1 for diatoms as a means to evaluate the consistency of both the final matrix and the autotrophic percentages of TChl *a* for the water column samples (Table A3). For the major pigments and autotrophic groups, the final matrix pigment ratios for the three analyses (diatom fuco:TChl *a* ratios of 0.35, 0.75, and 1.1) are generally ~99% similar. Further, the final autotrophic percentages for the individual samples are also ~99% similar for the three analyses with varying fuco:TChl *a* ratios for diatoms.

3. Results

a. Mixed-layer hydrography

For the regions assigned in this study, the average mixed-layer depth (defined as the depth at which $\sigma_{t(z)}$ exceeds the 0–5 m averaged σ_t by 0.1 kg m^{-3}; E. D. Cokelet, personal communication) ranged from 23 to 46 m during spring cruises and 17 to 29 m during summer cruises (Table A4). The mixed layer is consistently colder during spring with regional averages of −1.40°C to 1.92°C and 3.43°C to 6.05°C for spring and summer cruises, respectively. Average salinity values are indistinguishable between spring and summer (regional averages of 31.16% to 32.75%). Mixed-layer DO averages are greater in spring for all but region 1. Spring averages ranged from 329.75 to 384.42 μmol kg^{-1}, and summer averages varied from 312.84 to 347.94 μmol kg^{-1}. The northern and coastal regions (1, 3, and 4) are undersaturated with respect to DO in spring, most likely due to the recent ice cover. Region 2, encompassing the northern outer shelf and St. Matthew Island, is slightly oversaturated (Table A4), which may be attributed to the enhanced primary production observed during HLY0902 in this area. Average percent ice cover at a given station is estimated as the 7-day mean ice cover for the period of time preceding the sampling day using data from Advanced Microwave Scanning Radiometer–Earth Observing System Sensor on the NASA Aqua Satellite (Cavalieri, Markus, and Comiso 2014). Mean sea-ice concentrations were determined in a box (0.15° latitude by 0.3° longitude) surrounding each CTD station (S. A. Salo, personal communication). For the shelf regions (1–5), percent ice cover, averaged by cruise, ranges from open-water conditions (no ice) to 69 ± 48% ice cover. For the spring cruises, many of the ice-covered stations were occupied during HLY0802 (2008) and HLY0902 (2009), whereas most were ice free during TN249 (2010) as this cruise occurred later in the spring.

b. Water column pigment and POM concentrations

Average concentrations of TChl *a* were greater in spring than in summer for all regions. The exception is region 3, which may be the result of limited sampling and ~98% ice cover during the collection of one of the two profiles in this region (Table A4; Table 2). The relatively high average TChl *a* concentration in region 2 during the spring is due to frequent sampling of an MIZ bloom in 2009 (Fig. 1, gray boxes) (Lomas et al. 2012).

Table 2. Regional averages of primary pigment concentrations ($\mu g\ L^{-1}$) in the upper water column: total chlorophyll *a* (TChl *a*), fucoxanthin, total chlorophyll *b* (TChl *b*), 19′-hexanoyloxyfucoxanthin (19′-Hex), phaeophytin *a*, and phaeophorbide *a*.

Region	TChl *a* $\mu g\ L^{-1}$	Fucoxanthin $\mu g\ L^{-1}$	TChl *b* $\mu g\ L^{-1}$	19′-Hex $\mu g\ L^{-1}$	Phaeophytin *a* $\mu g\ L^{-1}$	Phaeophorbide *a* $\mu g\ L^{-1}$
Spring						
1	0.740 ± 1.473	0.258 ± 0.564	0.019 ± 0.019	0.003 ± 0.005	0.014 ± 0.028	0.029 ± 0.071
2	8.868 ± 10.924	3.591 ± 4.304	0.024 ± 0.020	0.003 ± 0.002	0.136 ± 0.133	0.628 ± 1.380
3	0.224 ± 0.189	0.077 ± 0.078	0.016 ± 0.006	0.001 ± 0.000	0.016 ± 0.010	0.031 ± 0.028
4	1.725 ± 2.420	0.727 ± 1.202	0.031 ± 0.035	0.003 ± 0.003	0.059 ± 0.143	0.425 ± 1.208
5	5.261 ± 3.764	2.100 ± 1.810	0.050 ± 0.020	0.004 ± 0.004	0.074 ± 0.060	0.359 ± 0.076
6	4.721 ± 6.356	2.030 ± 2.838	0.026 ± 0.018	0.019 ± 0.020	0.142 ± 0.190	0.434 ± 0.595
7	1.735 ± 1.532	0.683 ± 0.630	0.096 ± 0.067	0.023 ± 0.018	0.018 ± 0.014	0.419 ± 0.412
Summer						
1	0.401 ± 0.970	0.152 ± 0.413	0.018 ± 0.017	0.003 ± 0.003	0.004 ± 0.009	0.016 ± 0.042
2	0.878 ± 1.149	0.164 ± 0.211	0.074 ± 0.056	0.177 ± 0.369	0.011 ± 0.021	0.030 ± 0.077
3	0.530 ± 0.213	0.159 ± 0.086	0.032 ± 0.021	0.006 ± 0.003	0.011 ± 0.009	0.043 ± 0.051
4	0.570 ± 0.368	0.127 ± 0.098	0.060 ± 0.042	0.025 ± 0.061	0.012 ± 0.015	0.038 ± 0.063
5	0.445 ± 0.384	0.128 ± 0.150	0.024 ± 0.019	0.008 ± 0.009	0.007 ± 0.007	0.053 ± 0.075
6	0.581 ± 0.332	0.084 ± 0.061	0.032 ± 0.022	0.163 ± 0.140	0.009 ± 0.010	0.007 ± 0.011
7	0.538 ± 0.310	0.116 ± 0.069	0.040 ± 0.050	0.041 ± 0.032	0.014 ± 0.012	0.027 ± 0.020

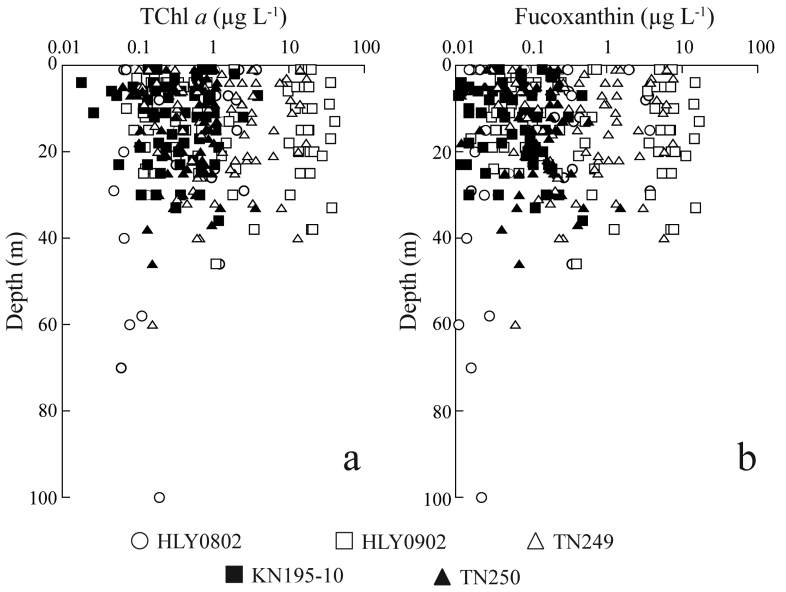

Figure 2. Depth profiles of total chlorophyll *a* (TChl *a*) (a) and fucoxanthin (b) (μg L^{-1}). Open (spring) and shaded (summer) symbols correspond to specific cruises listed in the symbol key in the figure.

Depth-averaged concentrations of TChl *a* commonly exceed 1 μg L^{-1} during the spring cruises. At only four stations during this field program did the depth-averaged concentration of TChl *a* exceed 5 μg L^{-1} (Fig. 2a), which signifies a bloom condition. These stations were BL (region 2), which was sampled multiple times during HLY0902, MN19 (region 6), NP14 (region 5), and HBR1 (region 4) during TN249 (Fig. 1, gray-shaded symbols). These bloom stations were responsible for the overall high TChl *a* averages in these regions (Table 2). The most abundant indicator pigment associated with the TChl *a* is fucoxanthin, and these two pigments are highly correlated ($m = 0.401x$, $r^2 = 0.978$, $P < 0.001$; Fig. 3a). There was greater variability in the relationship at stations exhibiting lower TChl *a* concentrations, particularly in summer. As with TChl *a* concentrations, the spatial distribution of fucoxanthin demonstrated substantial variability, ranging from <0.1 μg L^{-1} to >15 μg L^{-1}. Fucoxanthin concentrations exceeding 1 μg L^{-1} are generally associated with the spring bloom stations. No significant relationship exists between TChl *a* and either total chlorophyll *b* (TChl *b*; marker of chlorophytes) or 19′-hexanoyloxyfucoxanthin (19′-Hex; marker of prymnesiophytes); however, both of these accessory pigments were present at relatively higher concentrations when TChl *a* was low. The Σphaeopigment concentrations for particles in the upper water column were low, typically present at levels an order of magnitude less than TChl *a*.

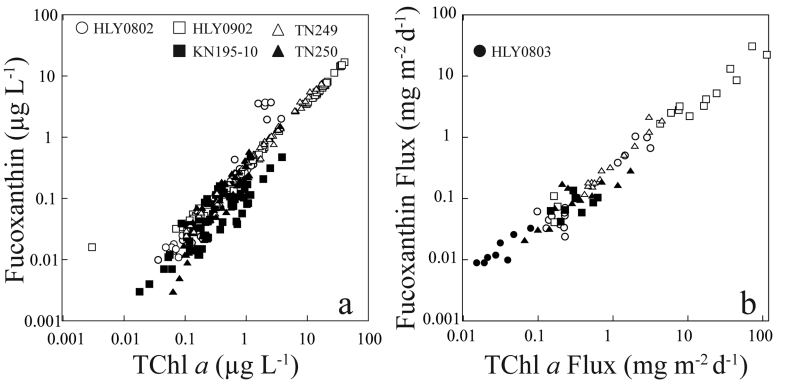

Figure 3. Relationship between water column concentrations (a) and sediment trap fluxes (b) of total chlorophyll *a* (TChl *a*) and fucoxanthin (a, μg L^{-1}; b, mg m^{-2} d^{-1}).

On a station-by-station basis, average upper water column POC and PON concentrations ranged from <7 to >120 μmol C L^{-1} and 1 to 11 μmol N L^{-1} during the spring cruises (Table 3). During summer, depth-averaged POC and PON concentrations were considerably lower ranging from 6 to 17 μmol C L^{-1} and 1 to 3 μmol N L^{-1} (Table 3). In both spring and summer 2010, average POP concentrations were >0.7 μmol P L^{-1} for all stations. Included with data from 2010, average bSi concentrations from the bloom station (BL) in 2009 were compared with the 2010 values (Table 3). Depth-averaged bSi concentrations ranged from <1 μmol Si L^{-1} at stations exhibiting low POC and PON concentrations to >10 μmol Si L^{-1} for stations with bloom condition levels of TChl *a* and elevated POC and PON concentrations.

c. Pigment and POM fluxes

The geographic patterns observed in the magnitude of the TChl *a* flux (mg m^{-2} d^{-1}) were similar to that of pigments in the overlying water column (Fig. 1 and Table 4). Specifically, the highest TChl *a* fluxes were associated with areas of the highest TChl *a* standing stock in the spring, such as those observed at station BL during HLY0902 and MN19 during TN249. Although fluxes of TChl *a* at times exceeded 20 mg m^{-2} d^{-1} at bloom stations, vertical fluxes over the upper 100 m are generally <2 mg m^{-2} d^{-1} at nonbloom stations for both spring and summer cruises. As with water column accessory pigments, fucoxanthin was the most abundant indicator pigment in vertically exported particulate material. The vertical flux of fucoxanthin was greatest at stations that exhibited elevated water column concentrations and vertical fluxes of TChl *a* (Table 4). The linear regression of fucoxanthin and TChl *a*in sinking particles ($m = 0.259x, r^2 = 0.863, P < 0.001$; Fig. 3b) demonstrates a lower slope than the water column–suspended particles. However, the mean ratios (mean = 0.33 ± 0.35 for water column particles; 0.35 ± 0.14 for sinking particles) are statistically

Table 3. Station averages of upper water column concentrations (μmol L^{-1}) of particulate organic carbon (POC), particulate organic nitrogen (PON), particulate organic phosphorus (POP), and biogenic silica (bSi).

Station no. Station ID	n	POC μmol L^{-1}	PON μmol L^{-1}	POP μmol L^{-1}	bSi μmol L^{-1}
HLY0902					
85 BL15	7				8.20 ± 3.30
90 BL20	7				11.75 ± 1.51
115 BL21	7				18.47 ± 6.83
TN249					
7 NP12	3				1.96 ± 0.37
24 Z15	3	70.06 ± 18.53	5.88 ± 2.53		10.85 ± 3.30
39 IE1	3	39.40 ± 13.40	3.74 ± 1.45		6.79 ± 4.72
49 MN19	4	62.05 ± 60.89	5.35 ± 4.67		16.03 ± 4.79
50 MN19	3	126.60 ± 7.15	10.89 ± 0.47		
55 NZ11.5	7	6.58 ± 2.86	1.09 ± 0.42	0.08 ± 0.02	1.27 ± 0.38
66 NZ4.5	3	56.40 ± 6.44	3.19 ± 0.54	0.34 ± 0.03	9.02 ± 0.68
71 HBR1	3	100.32 ± 56.58	7.27 ± 3.57	0.69 ± 0.14	16.03 ± 3.61
81 70M26	3	21.93 ± 2.16	1.25 ± 0.19	0.17 ± 0.03	5.48 ± 0.91
87 CN17	7	20.84 ± 10.17	1.43 ± 5.29	0.35 ± 0.12	2.93 ± 1.37
99 70M4	3	46.11 ± 33.62	5.81 ± 4.10		6.49 ± 0.51
124 70M29	3	9.97 ± 4.45	1.75 ± 0.32	0.13 ± 0.01	1.89 ± 0.92
147 70M52	3	15.17 ± 14.70	2.63 ± 2.42	0.20 ± 0.14	2.95 ± 2.72
156 SL12	3	10.96 ± 11.61	1.31 ± 1.56	0.17 ± 0.12	1.82 ± 1.50
163 MN19	7	29.38 ± 14.83	3.16 ± 2.30	0.24 ± 0.17	1.80 ± 0.80
175 MN8	3	11.15 ± 2.00	1.54 ± 0.23	0.21 ± 0.13	1.49 ± 0.73
179 NP3	7	11.43 ± 3.04	1.96 ± 0.45	0.16 ± 0.06	1.58 ± 0.95
TN250					
8 UAP5	4	12.93 ± 1.62	1.82 ± 0.20	0.22 ± 0.05	1.55 ± 0.06
20 CN8	3	12.05 ± 5.24	2.55 ± 1.08	0.14 ± 0.05	2.07 ± 1.91
25 CN17	7	11.57 ± 1.43	2.39 ± 0.23	0.26 ± 0.10	1.02 ± 0.14
32 CNN4	3	15.26 ± 1.88	2.36 ± 0.76	0.21 ± 0.03	1.69 ± 1.16
47 NP9	3	16.94 ± 5.41	1.79 ± 1.58	0.14 ± 0.01	1.79 ± 1.76
53 TD2	6	13.60 ± 4.18	1.82 ± 0.67	0.19 ± 0.05	0.90 ± 0.28
67 TR3	7	11.20 ± 3.17	1.12 ± 0.28	0.11 ± 0.02	0.33 ± 0.06
82 MN1	3	14.57 ± 0.57	1.98 ± 0.20	0.27 ± 0.04	5.55 ± 0.99
97 MN16	3	14.24 ± 10.70	2.02 ± 1.79	0.26 ± 0.31	1.22 ± 1.73
103 TR4	6	11.65 ± 4.13	2.08 ± 1.06	0.17 ± 0.08	1.11 ± 0.33
122 ML3	3	5.52 ± 13.72	1.94 ± 1.46	0.14 ± 0.08	1.68 ± 2.15
145 BN3	4	6.82 ± 2.39	1.33 ± 0.80	0.08 ± 0.01	0.29 ± 0.06
167 70M39	3	8.52 ± 0.93	1.16 ± 0.24	0.07 ± 0.02	0.88 ± 1.05
197 70M9	3	12.27 ± 2.45	2.16 ± 0.90	0.17 ± 0.09	1.25 ± 1.53

Table 4. Sediment trap profiles of primary pigment (mg m^{-2} d^{-1}) and particulate fluxes (mmol m^{-2} d^{-1}): total chlorophyll *a* (TChl *a*), fucoxanthin, phaeophytin *a*, phaeophorbide *a*, particulate organic carbon (POC), particulate organic nitrogen (PON), particulate organic phosphorus (POP), and biogenic silica (bSi). POC export fluxes from Baumann, Moran, Lomas, et al. (2013).

Station/depth m	TChl *a* mg m^{-2} d^{-1}	Fucoxanthin mg m^{-2} d^{-1}	Phaeophytin *a* mg m^{-2} d^{-1}	Phaeophorbide *a* mg m^{-2} d^{-1}	POC mmol m^{-2} d^{-1}	PON mmol m^{-2} d^{-1}	POP mmol m^{-2} d^{-1}	bSi mmol m^{-2} d^{-1}
HLY0802								
T1-25	0.194	0.038	0.006	0.026	1.92	0.49	–	–
40	0.226	0.053	0.007	0.039	1.67	0.43	–	–
50	0.224	0.059	0.009	0.047	4.94	0.72	–	–
60	0.227	0.071	0.011	0.052	2.02	0.49	–	–
100	0.138	0.045	0.007	0.039	4.05	0.72	–	–
T2-25	0.221	0.034	0.005	0.020	7.58	1.35	–	–
40	0.097	0.062	0.002	0.014	3.03	0.69	–	–
50	0.227	0.024	0.007	0.030	5.20	1.01	–	–
60	0.128	0.033	0.002	0.014	3.39	0.69	–	–
100	0.151	0.052	0.012	0.025	4.22	0.75	–	–
T3-25	2.832	1.007	0.369	3.997	8.91	0.60	–	–
40	1.980	1.042	0.155	2.583	7.67	1.35	–	–
50	3.145	0.671	0.390	6.086	7.37	1.29	–	–
60	1.150	0.388	0.105	1.489	6.21	1.18	–	–
100	1.436	0.509	0.099	2.988	5.36	1.15	–	–
HLY0803								
PIT1-40	0.015	0.009	0.153	0.194	22.30	3.04	–	–
60	0.019	0.009	0.134	0.172	14.43	2.07	–	–
100	0.015	0.009	0.102	0.173	19.14	2.48	–	–
PIT2-40	0.039	0.010	0.010	0.091	9.00	1.27	–	–
60	0.027	0.012	0.009	0.084	9.57	1.21	–	–
100	0.021	0.011	0.010	0.065	8.17	0.95	–	–
PIT3-40	0.079	0.033	0.026	0.592	14.52	2.02	–	–
60	0.047	0.026	0.030	0.458	13.44	1.93	–	–
100	0.031	0.019	0.018	0.183	7.98	0.96	–	–

(Continued)

Table 4. (Continued)

Station/depth m	TChl *a* mg m^{-2} d^{-1}	Fucoxanthin mg m^{-2} d^{-1}	Phaeophytin *a* mg m^{-2} d^{-1}	Phaeophorbide *a* mg m^{-2} d^{-1}	POC mmol m^{-2} d^{-1}	PON mmol m^{-2} d^{-1}	POP mmol m^{-2} d^{-1}	bSi mmol m^{-2} d^{-1}
HLY0902								
NP15-25	0.165	0.041	0.009	0.058	9.64	1.47	–	–
50	0.182	0.074	0.014	0.099	10.52	1.52	–	–
100	0.163	0.110	0.020	0.105	11.00	1.19	–	–
BL2-25	36.886	13.205	0.723	3.911	46.56	7.91	–	–
50	7.570	2.795	0.247	1.788	17.07	2.55	–	–
100	4.275	1.671	0.152	1.149	28.55	3.65	–	–
BL15-25	113.536	22.407	1.532	7.405	66.30	10.92	–	9.58
50	17.558	4.182	0.255	1.548	36.46	5.19	–	6.86
100	24.258	5.242	0.354	1.833	40.89	5.46	–	10.27
BL15-1-25	44.857	8.589	0.912	6.026	60.71	10.85	–	26.03
50	16.382	3.262	0.324	2.374	28.74	4.93	–	7.32
100	10.536	2.217	0.185	1.475	44.22	6.19	–	45.35
B:21-25	72.354	30.664	1.071	13.837	272.91	40.32	–	–
50	7.761	3.214	0.202	1.778	77.64	9.64	–	–
100	5.954	2.513	0.214	1.656	108.15	13.92	–	–
KN195-10								
CN17-25	0.543	0.086	0.067	0.343	42.10	4.32	–	–
50	0.623	0.104	0.103	0.858	40.64	4.19	–	–
100	0.383	0.059	0.062	0.564	38.54	3.74	–	–
NP15-25	0.147	0.063	0.052	0.714	25.31	3.75	–	–
50	0.200		0.142	0.992	48.12	5.00	–	–
100	0.229	0.065	0.132	1.071	29.60	2.45	–	–
P14-7-25	0.326	0.101	0.155	0.939	20.58	2.97	–	–
50	0.314	0.103	0.283	1.332	21.89	2.57	–	–
100	0.295	0.136	0.224	2.140	23.11	2.65	–	–

(Continued)

Table 4. (Continued)

Station/depth m	TChl *a* mg m^{-2} d^{-1}	Fucoxanthin mg m^{-2} d^{-1}	Phaeophytin *a* mg m^{-2} d^{-1}	Phaeophorbide *a* mg m^{-2} d^{-1}	POC mmol m^{-2} d^{-1}	PON mmol m^{-2} d^{-1}	POP mmol m^{-2} d^{-1}	bSi mmol m^{-2} d^{-1}
TN249								
MN19-25	3.024	2.169	1.576	9.565	73.71	8.97	–	46.21
50	4.512	1.886	1.929	7.941	43.50	6.16	–	34.27
100	3.052	1.239	1.561	4.933	48.07	5.91	–	42.18
NZ11.5-25	0.525	0.175	0.171	0.607	19.35	3.76	0.12	18.81
50	0.529	0.157	0.283	0.714	20.29	3.96	0.12	17.72
100	0.518	0.186	0.309	0.583	11.55	2.74	0.11	24.36
CN17-25	1.951	0.729	0.156	7.360	39.47	6.48	0.22	18.53
50	0.566	0.183	0.077	5.251	15.27	2.79	0.23	11.81
100	0.464	0.162	0.073	3.067	2.71	1.17	0.24	9.95
MN19-2-25	0.704	0.289	0.143	1.243	15.48	2.49	0.36	10.55
50	0.669	0.208	0.200	1.578	15.75	2.95	0.11	8.49
100	0.416	0.119	0.158	1.187	13.58	2.61	0.07	8.28
NP14-25	1.403	0.522	0.146	16.700	24.62	5.40	0.11	42.41
50	0.917	0.326	0.090	10.941	2.08	1.62	0.16	26.07
100	0.466	0.184	0.063	7.844	4.71	3.03	0.06	21.17
TN250								
CN17-25	0.524	0.112	0.065	0.210	113.45	14.15	0.54	7.14
50	1.158	0.166	0.275	0.785	81.04	8.98	0.43	11.36
100	1.713	0.287	0.426	1.810	69.12	7.38	0.42	18.40
NP14-25	0.283	0.084	0.066	0.182	30.64	3.01	0.19	6.25
50	0.365	0.095	0.089	0.488	30.50	2.22	0.22	6.75
100	0.707	0.189	0.217	1.784	39.58	3.12	0.07	21.56
P14-7-25	0.099	0.031	0.020	0.075	21.72	2.47	0.04	1.69
50	0.066	0.021	0.041	0.166	15.48	1.41	0.15	3.65
100	0.141	0.032	0.055	0.176	19.11	1.09	0.10	1.82
MN19-25	0.167	0.070	0.088	0.065	24.89	2.89	0.15	4.38
50	0.209	0.174	0.394	0.002	17.26	1.83	0.03	5.04
100	0.250	0.150	0.889	0.001	11.83	1.00	0.23	5.98

(Continued)

Table 4. (Continued)

Station/depth m	TChl *a* mg m^{-2} d^{-1}	Fucoxanthin mg m^{-2} d^{-1}	Phaeophytin *a* mg m^{-2} d^{-1}	Phaeophorbide *a* mg m^{-2} d^{-1}	POC mmol m^{-2} d^{-1}	PON mmol m^{-2} d^{-1}	POP mmol m^{-2} d^{-1}	bSi mmol m^{-2} d^{-1}
KN195-10								
CN17-25	0.543	0.086	0.067	0.343	42.10	4.32	–	–
50	0.623	0.104	0.103	0.858	40.64	4.19	–	–
100	0.383	0.059	0.062	0.564	38.54	3.74	–	–
NP15-25	0.147	0.063	0.052	0.714	25.31	3.75	–	–
50	0.200		0.142	0.992	48.12	5.00	–	–
100	0.229	0.065	0.132	1.071	29.60	2.45	–	–
P14-7-25	0.326	0.101	0.155	0.939	20.58	2.97	–	–
50	0.314	0.103	0.283	1.332	21.89	2.57	–	–
100	0.295	0.136	0.224	2.140	23.11	2.65	–	–
TN249								
MN19-25	3.024	2.169	1.576	9.565	73.71	8.97	–	46.21
50	4.512	1.886	1.929	7.941	43.50	6.16	–	34.27
100	3.052	1.239	1.561	4.933	48.07	5.91	–	42.18
NZ11.5-25	0.525	0.175	0.171	0.607	19.35	3.76	0.12	18.81
50	0.529	0.157	0.283	0.714	20.29	3.96	0.12	17.72
100	0.518	0.186	0.309	0.583	11.55	2.74	0.11	24.36
CN17-25	1.951	0.729	0.156	7.360	39.47	6.48	0.22	18.53
50	0.566	0.183	0.077	5.251	15.27	2.79	0.23	11.81
100	0.464	0.162	0.073	3.067	2.71	1.17	0.24	9.95
MN19-2-25	0.704	0.289	0.143	1.243	15.48	2.49	0.36	10.55
50	0.669	0.208	0.200	1.578	15.75	2.95	0.11	8.49
100	0.416	0.119	0.158	1.187	13.58	2.61	0.07	8.28
NP14-25	1.403	0.522	0.146	16.700	24.62	5.40	0.11	42.41
50	0.917	0.326	0.090	10.941	2.08	1.62	0.16	26.07
100	0.466	0.184	0.063	7.844	4.71	3.03	0.06	21.17

(Continued)

Table 4. (Continued)

Station/depth m	TChl *a* mg m^{-2} d^{-1}	Fucoxanthin mg m^{-2} d^{-1}	Phaeophytin *a* mg m^{-2} d^{-1}	Phaeophorbide *a* mg m^{-2} d^{-1}	POC mmol m^{-2} d^{-1}	PON mmol m^{-2} d^{-1}	POP mmol m^{-2} d^{-1}	bSi mmol m^{-2} d^{-1}
TN250								
CN17-25	0.524	0.112	0.065	0.210	113.45	14.15	0.54	7.14
50	1.158	0.166	0.275	0.785	81.04	8.98	0.43	11.36
100	1.713	0.287	0.426	1.810	69.12	7.38	0.42	18.40
NP14-25	0.283	0.084	0.066	0.182	30.64	3.01	0.19	6.25
50	0.365	0.095	0.089	0.488	30.50	2.22	0.22	6.75
100	0.707	0.189	0.217	1.784	39.58	3.12	0.07	21.56
P14-7-25	0.099	0.031	0.020	0.075	21.72	2.47	0.04	1.69
50	0.066	0.021	0.041	0.166	15.48	1.41	0.15	3.65
100	0.141	0.032	0.055	0.176	19.11	1.09	0.10	1.82
MN19-25	0.167	0.070	0.088	0.065	24.89	2.89	0.15	4.38
50	0.209	0.174	0.394	0.002	17.26	1.83	0.03	5.04
100	0.250	0.150	0.889	0.001	11.83	1.00	0.23	5.98

similar, which suggests that material sinking from the photic zone is similar in composition to the autotrophic community with respect to fucoxanthin-containing POM (Fig. 3b). The presence of TChl *b* and 19′-Hex was occasionally detected in settling material, though typically to a lesser extent than their relative concentration in the overlying water column (Table 4). The ratio of Σphaeopigments to TChl *a* (Σphaeo:TChl *a*) in sinking particles was usually >1, indicating that material sinking through the water column is at least partly degraded due to the presence of senescent cells or zooplankton fecal pellets (Table 4).

Sediment trap POC fluxes determined during this field campaign have been presented elsewhere (Moran et al. 2012; Baumann, Moran, Lomas, et al. 2013). A subset of values used for the present analysis is listed in Table 4. Briefly, POC fluxes along the shelf break and in open water were relatively low in early spring during HLY0802 and HLY0902 (NP15), whereas those over the outer shelf at station BL represented some of the highest fluxes measured in this study. POC fluxes increased in late spring (TN249) and early summer (KN195-10 and TN250) and decreased by midsummer (HLY0803). The seasonal succession of the PON flux showed a similar temporal progression as POC export, with low early spring fluxes that increased throughout the spring and early summer (Table 4). POP fluxes were <1 mmol P m^{-2} d^{-1}, with the higher fluxes associated with the higher rates of POC and PON export (Table 4). No significant correlation was found between the flux of bSi with either POC or TChl *a* export. The bSi fluxes below the mixed layer were <20 mmol Si m^{-2} d^{-1} for most stations, whereas fluxes >40 mmol Si m^{-2} d^{-1} were measured at bloom stations BL (HLY0902) and MN19 (TN249).

4. Discussion

a. Description of the autotrophic community and vertical export

The observation of a predominantly diatom autotrophic community in the spring and in the MIZ is consistent with previous and concurrent studies of the ice-edge population (Schandelmeier and Alexander 1981; Moran et al. 2012) and the presence of abundant resting stage cells in the underlying sediment in this region (Tsukazaki et al. 2013). In this study, diatoms represent a range of 71.5 ± 10.8% to 95.7 ± 2.1% (regional mean ±1σ) of TChl *a* for regions 1–5 over the shelf. The contribution of diatoms to TChl *a* in the northern (region 6) and southern (region 7) regions of the shelf break is on average 80.0 ± 18.6% and 65.8 ± 26.5%, respectively (Table 5). Throughout the shelf and shelf break, other algal classes, namely prymnesiophytes, chlorophytes, cryptophytes, and cyanobacteria, are present, but to a much lesser degree relative to diatoms in spring (Table 5).

A seasonal shift in the autotrophic community is apparent from the upper–water column pigment distribution. During summer cruises, the shelf and shelf break exhibit lower TChl *a* levels and a heterogeneous phytoplankton assemblage. Algal classes present in relatively smaller proportions during spring are key contributors to TChl *a* in early summer (Table 5). Specifically, prymnesiophytes emerge along the shelf break comprising 54.5 ± 32.3% and 27.1 ± 23.2% of the TChl *a* in regions 6 and 7, respectively. Together with prymnesiophytes,

Table 5. Regional averages of percent contribution by algal group to total chlorophyll *a*.

Region	Diatoms	Prymnesiophytes	Pelagophytes	Chlorophytes	Prasinophytes	Cryptophytes	Dinoflagellates	Cyanobacteria
Spring								
1	77.57 ± 17.67	2.91 ± 3.31	1.91 ± 2.11	9.96 ± 10.74	1.36 ± 1.58	4.07 ± 3.15	1.70 ± 1.89	0.52 ± 0.64
2	88.01 ± 18.43	1.61 ± 2.78	1.16 ± 2.10	4.35 ± 6.67	1.06 ± 2.10	2.34 ± 3.55	1.12 ± 1.85	0.34 ± 0.74
3	71.45 ± 10.77	1.23 ± 0.53	2.41 ± 1.20	12.44 ± 3.55	0.84 ± 0.41	7.18 ± 3.56	2.92 ± 3.25	1.53 ± 1.16
4	85.38 ± 14.17	1.83 ± 2.76	0.95 ± 0.83	7.22 ± 7.51	0.83 ± 1.04	2.69 ± 2.36	0.83 ± 0.85	0.28 ± 0.44
5	95.67 ± 2.08	0.29 ± 0.03	0.18 ± 0.28	1.96 ± 0.97	0.20 ± 0.06	1.47 ± 0.90	0.17 ± 0.05	0.06 ± 0.06
6	79.95 ± 18.63	7.77 ± 8.86	2.11 ± 2.45	4.94 ± 4.42	0.62 ± 0.90	3.02 ± 3.45	1.47 ± 1.91	0.12 ± 0.17
7	65.79 ± 26.53	5.58 ± 3.85	1.96 ± 1.43	19.11 ± 16.61	1.03 ± 1.41	4.08 ± 2.51	2.17 ± 1.40	0.28 ± 0.41
Summer								
1	50.21 ± 34.72	6.66 ± 6.10	2.73 ± 2.39	27.11 ± 23.77	2.35 ± 2.43	6.51 ± 7.65	2.34 ± 1.85	2.10 ± 2.16
2	37.83 ± 24.10	18.52 ± 28.38	1.61 ± 1.70	34.94 ± 26.32	1.99 ± 2.64	3.14 ± 2.26	1.55 ± 2.60	0.42 ± 0.55
3	74.44 ± 10.48	4.31 ± 4.62	4.06 ± 4.13	9.10 ± 3.48	2.73 ± 1.61	3.70 ± 2.32	1.10 ± 1.46	0.56 ± 0.77
4	54.38 ± 26.01	12.87 ± 25.73	2.01 ± 1.99	22.30 ± 16.81	3.25 ± 4.07	3.31 ± 3.73	1.40 ± 1.65	0.47 ± 0.88
5	63.44 ± 23.73	5.47 ± 6.32	1.46 ± 1.81	17.95 ± 17.69	2.12 ± 3.29	6.92 ± 7.27	2.42 ± 3.66	0.23 ± 0.25
6	24.43 ± 20.62	54.48 ± 31.09	3.02 ± 1.09	13.53 ± 18.08	0.68 ± 0.85	3.04 ± 3.71	0.57 ± 0.55	0.25 ± 0.29
7	49.46 ± 28.58	27.11 ± 23.23	3.01 ± 2.10	9.18 ± 10.95	1.66 ± 1.89	8.39 ± 8.16	0.71 ± 0.49	0.49 ± 0.49

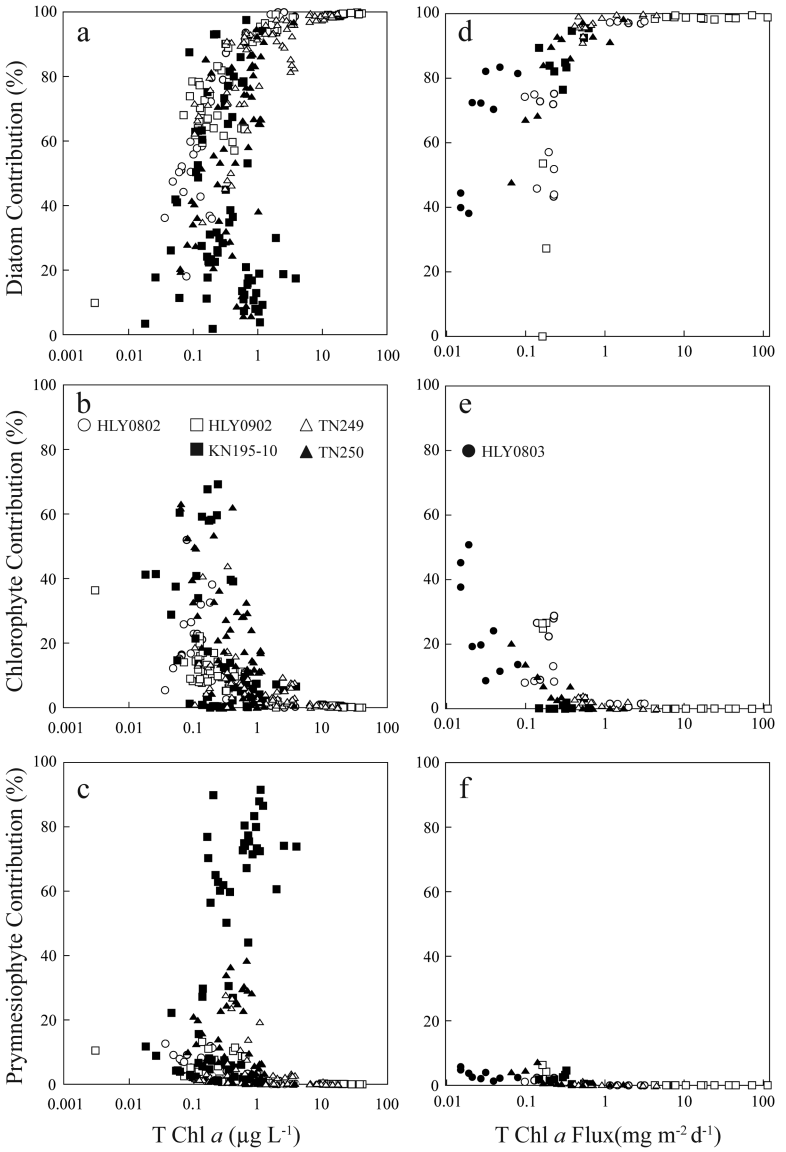

Figure 4. Percent contribution to ambient total chlorophyll *a* (TChl *a*) (a–c) and TChl *a* flux (d–f) for diatoms (a and d), chlorophytes (b and e), and prymnesiophytes (c and f). There are no summer 2008 (HLY0803) water column data, only particle flux data.

chlorophytes and cryptophytes also become important contributors to TChl *a* in the shelf and shelf-break regions in summer (Table 5).

Diatoms are responsible primarily for the elevated levels of TChl *a* (e.g., >5 µg L^{-1}) in the spring, particularly at the bloom stations (Fig. 4a), whereas chlorophytes and

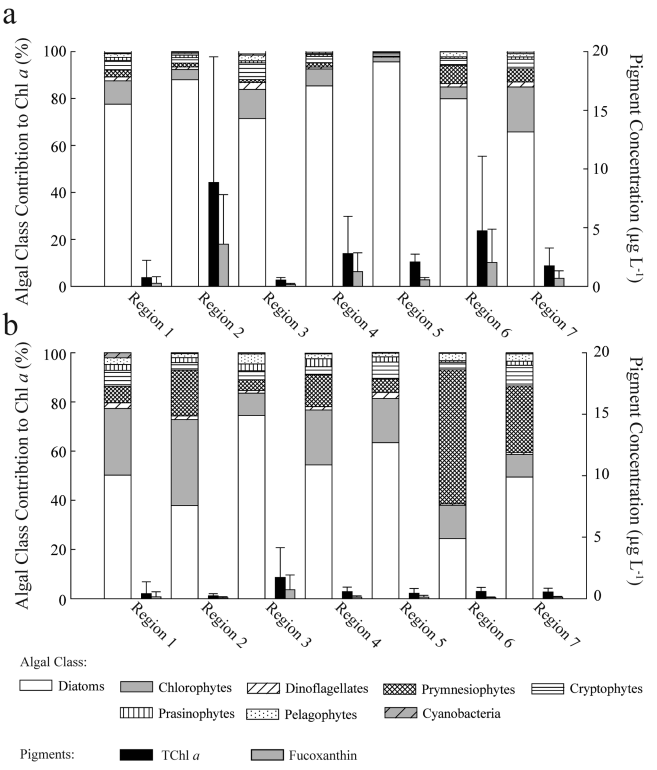

Figure 5. Average algal class contribution to autotrophic community (%) by region for spring (a) and summer (b). Thin bars represent average total chlorophyll *a* (TChl *a*) (black) and fucoxanthin (gray) concentrations and correspond to the right vertical axes.

prymnesiophytes are typically not present during this period (Fig. 4b and c). This trend holds at lower TChl *a* (e.g., <1 μg L^{-1}) concentrations, in both spring and summer, as diatoms frequently still represent the major autotrophic contribution (Fig. 4a). However, when the relative contribution of diatoms is low during the summer, chlorophytes and prymnesiophytes dominate the autotrophic community (Fig. 4b and c). Key differences with respect to the autotrophic community are evident in the early summer autotrophic communities between 2009 (KN195-10) and 2010 (TN250). A number of stations in 2009, especially in regions 6 and 7, are characterized by high contributions of prymnesiophytes to the TChl *a* (Table 5; Fig. 5). By contrast, in 2010, the autotrophic community is composed primarily of diatoms and chlorophytes, whereas there is little contribution from prymnesiophytes at these same stations along the shelf break (Fig. 4c). It is not known what factors may be responsible for the differences in the phytoplankton community structure between 2009 and 2010 because sampling dates overlap, and hydrographic properties such as, average mixed-layer depths, DO concentrations, upper–water column temperatures, and TChl *a* concentrations show little interannual variability.

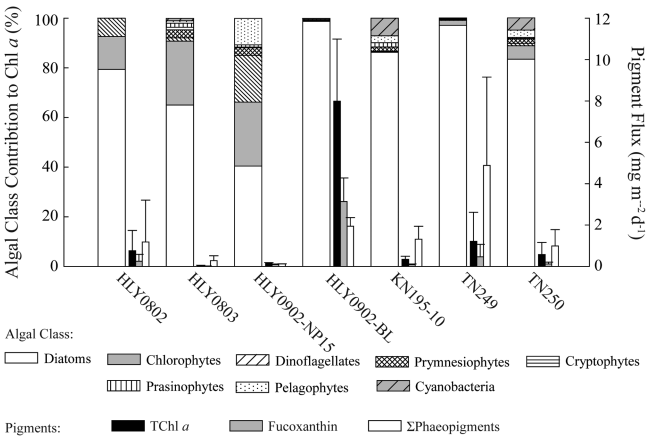

Figure 6. Phytoplankton composition (%) of the vertical flux of particulate organic matter by cruise. Thin bars represent average total chlorophyll *a* (TChl *a*) (black), fucoxanthin (gray), and total phaeopigments (Σphaeopigments) (white) and correspond to the right vertical axes.

As with the geographic distribution of the phytoplankton assemblage in the water column, diatoms also dominate export in the form of particles sinking from the photic zone (Figs. 5 and 6). On a station-by-station basis, there is little vertical variability in the percent composition of the major algal classes in exported particles. However, both TChl *a* and POC fluxes vary substantially over the upper 100 m (Table 6), suggesting nonpreferential consumption and remineralization of sinking particles. At three locations, all of which are in region 7 (PIT1-HLY0803) or the southern reach of region 6 (T1-HLY0802 and NP15-HLY0902), the average composition of the vertical flux is <50% diatoms. The relatively low diatom contribution at stations T1 and NP15 is associated with low TChl *a* and POC fluxes (Table 6). Interestingly, the average POC flux at PIT1 is the highest observed in summer 2008, whereas the average TChl *a* flux at this station is the lowest measured during the entire field program. At these stations, other algal classes, namely chlorophytes, pelagophytes, and dinoflagellates, represent the largest fraction of the sinking phytoplankton assemblage. Apart from these few stations, the observed shift in the autotrophic community in the water column is not reflected in the phytoplankton composition of exported particles (Tables 5 and 6; Fig. 6). For all other stations in regions 2 (BL), 6, and 7, diatoms represent at least 70% of the vertical flux of TChl *a*. This indicates that, regardless of the TChl *a* and POC flux from the photic zone, diatoms are the primary algal class exported from the photic zone (Fig. 6).

The magnitude and seasonal progression of the POC export flux, combined with differences in the ratio of Σphaeo:TChl *a* between the upper water column and in sinking particles, provides important insights into the mechanisms controlling the export of diatoms from the photic zone. As noted previously, POC along the shelf break exhibits a progressive increase

Table 6. Algal group percent contribution to the flux of total chlorophyll *a* through the water column.

Station/depth m	Diatoms	Prymnesiophytes	Pelagophytes	Chlorophytes	Prasinophytes	Cryptophytes	Dinoflagellates	Cyanobacteria
HLY0802								
T1-25	57.17	1.66	8.40	22.48	5.58	0.23	4.48	0
40	51.94	1.87	8.83	28.19	1.00	0.19	7.97	0
50	43.37	1.97	9.12	28.01	8.85	0.16	8.52	0
60	44.04	2.35	10.95	28.89	1.70	0.15	11.91	0
100	45.89	2.42	10.60	26.68	1.95	0.17	12.28	0
T2-25	72.03	1.68	4.01	13.24	0.93	0.22	7.61	0.29
40	74.32	1.14	2.06	8.15	1.09	0.07	12.44	0.73
50	75.26	1.60	3.56	8.46	0.50	0.14	10.49	0
60	75.07	1.59	3.40	8.67	0.74	0.15	10.38	0
100	72.90	1.50	4.30	9.05	0.59	0.07	11.59	0
T3-25	97.02	0.05	0.29	1.61	0.36	0.03	0.51	0.13
40	97.13	0.04	0.63	0.60	0.48	0.02	0.82	0.27
50	97.70	0.07	0.00	1.63	0.38	0.02	0.10	0.10
60	97.39	0.07	0.02	1.63	0.43	0.02	0.19	0.24
100	97.66	0.09	0.02	1.52	0.37	0.02	0.14	0.17
HLY0803								
PIT1-40	39.98	4.84	1.58	45.31	3.23	0.44	2.84	1.78
60	38.21	3.81	1.35	50.86	2.10	0.45	2.40	0.83
100	44.52	5.80	1.65	37.76	4.08	0.51	3.09	2.60
PIT2-40	70.44	1.36	0.67	24.23	0.99	0.90	1.12	0.29
60	72.35	2.14	0.88	19.84	2.61	1.10	0.97	0.12
100	72.51	2.59	1.10	19.35	1.80	0.61	1.35	0.70
PIT3-40	81.53	2.48	0.31	13.76	0	1.91	0	0
60	83.47	2.27	0.47	11.69	0	2.09	0	0
100	82.18	4.04	0.71	8.74	0	1.17	0.06	3.10

(Continued)

Table 6. (Continued)

Station/depth m	Diatoms	Prymnesiophytes	Pelagophytes	Chlorophytes	Prasinophytes	Cryptophytes	Dinoflagellates	Cyanobacteria
HLY0902								
NP15-25	53.60	1.90	7.66	24.83	0.73	0.20	11.08	0
50	27.27	4.21	13.81	26.64	1.09	0.30	26.67	0
100	0	6.33	20.07	26.43	1.42	0.26	45.50	0
BL2-25	98.67	0	0.01	0.07	0.42	0.00	0.44	0.40
50	98.91	0	0.01	0.06	0.42	0.01	0.14	0.45
100	98.44	0	0.02	0.04	0.34	0.02	0.09	1.05
BL15-25	98.84	0	0.02	0.07	0.39	0	0.39	0.29
50	98.44	0	0.02	0.09	0.49	0	0.49	0.47
100	98.23	0	0.02	0.09	0.54	0.01	0.51	0.60
BL15-1-25	98.60	0	0.01	0.07	0.40	0	0.49	0.42
50	98.65	0	0.02	0.06	0.41	0	0.47	0.38
100	98.80	0	0.03	0.04	0.34	0.01	0.35	0.43
B:21-25	99.54	0	0.03	0.01	0.17	0	0.13	0.12
50	99.51	0	0.03	0.01	0.15	0	0.21	0.09
100	98.98	0	0.03	0	0.46	0	0.22	0.30
KN195-10								
CN17-25	92.55	0.48	0.52	3.20	0.68	0.03	0.48	2.07
50	95.48	0.37	0.00	0.21	0.74	0.01	0.43	2.78
100	94.69	0.36	0.00	0.20	0.71	0.03	0.40	3.60
NP15-25	89.43	1.81	0.21	0.17	0.55	0.07	0.28	7.47
50	83.89	1.51	2.87	0	4.18	0.09	0.32	7.13
100	82.13	1.83	3.77	0	4.98	0.01	0.11	7.17
P14-7-25	83.37	4.59	2.77	1.90	0.77	0.05	1.28	5.26
50	84.87	3.25	3.29	0	0	0.06	0	8.53
100	76.44	2.50	6.53	1.08	0	0.07	0	13.39

(Continued)

Table 6. (Continued)

Station/depth m	Diatoms	Prymnesiophytes	Pelagophytes	Chlorophytes	Prasinophytes	Cryptophytes	Dinoflagellates	Cyanobacteria
TN249								
MN19-25	99.51	0.00	0.12	0.04	0.14	0.00	0.07	0.11
50	99.60	0.00	0.03	0.01	0.17	0.00	0.01	0.19
100	99.96	0.02	0.02	0.00	0.00	0.00	0.00	0
NZ11.5-25	91.06	1.30	0.03	3.61	0.67	0.05	2.02	1.25
50	93.10	0.71	0.02	4.08	0.50	0.05	1.36	0.19
100	95.51	0.48	0.04	1.99	0.36	0.03	1.38	0.21
CN17-25	97.64	0.11	0.01	2.18	0	0.05	0	0
50	95.88	0.24	0.01	3.73	0.03	0.11	0	0
100	95.79	0.24	0.02	3.74	0.09	0.11	0	0
MN19-2-25	97.21	0.11	0.04	2.06	0.23	0.03	0.15	0.16
50	96.59	0.24	0.00	2.15	0.20	0.04	0.65	0.12
100	96.45	0.53	0.00	2.95	0.00	0.07	0	0
NP14-25	99.76	0.17	0	0	0	0.07	0	0
50	98.80	0.20	0.00	0.96	0	0.05	0	0
100	99.23	0.18	0.01	0.52	0	0.06	0	0
TN250								
CN17-25	97.37	0.10	0	0.17	0.70	0.02	0.93	0.70
50	91.28	0.19	0	0.17	0.62	0.00	0.81	6.94
100	98.40	0.29	0	0.12	0.44	0.00	0.26	0.49
NP14-25	92.22	0.40	1.01	3.58	0.28	0.09	1.10	1.33
50	86.20	0.60	2.01	6.92	0.16	0.15	1.34	2.63
100	92.93	0.84	5.32	0	0.72	0.11	0.03	0.05
P14-7-25	67.17	4.55	6.62	13.72	0.89	0.24	4.23	2.58
50	47.74	4.11	6.26	20.21	0	0.67	3.83	17.19
100	68.43	7.23	7.33	9.91	0.67	0.19	0.37	5.86
MN19-25	84.07	0.66	1.17	6.97	1.08	0.09	2.66	3.30
50	89.78	0.73	1.82	3.50	0.26	0.08	0.98	2.86
100	92.89	0.49	1.29	2.72	0.22	0.05	0.09	2.24

in the magnitude of particle flux from early spring to late spring and early summer. Based on the observation that the POC flux increases from spring to summer, and that the export population is primarily diatoms (Fig. 6), particle export in early summer may be linked to the sinking of spring and MIZ primary production (Baumann, Moran, Lomas, et al. 2013). A temporal lag in the export of spring primary production as POC in summer has also been observed in other high-latitude systems (Rutgers van der Loeff, Friedrich, and Bathmann 1997; Dunbar, Leventer, and Mucciarone 1998; Asper and Smith 1999; Thibault et al. 1999). The average ratio of the Σphaeo:TChl *a* is >1 in material exported below the photic zone in late spring and early summer (50 m sediment traps; Table 4). In contrast, the Σphaeo:TChl *a* ratio in phytoplankton derived from integrated phaeopigment and TChl *a* stocks in the photic zone averages ∼0.1. The low ratio of the autotrophic population indicates an actively growing phytoplankton community (Bianchi et al. 2002). In comparison with phytoplankton in the photic zone, the Σphaeo:TChl *a* ratio in sinking particles is much greater than those in the upper water column (∼8–75 times greater), which indicates that sinking POM is composed of substantially degraded chlorophyll *a* and consists of a combination of senescent cells and zooplankton fecal pellets (Tables 2 and 4).

Phaeophorbide *a*, the degradation pigment resulting from metazoan digestion, represents ∼80% of the Σphaeopigment concentration in sinking particles (Table 4). This observation suggests that zooplankton grazing of spring primary production and subsequent sinking of fecal pellets is an important control on the vertical export of POC along the shelf break. Although microzooplankton abundance and grazing pressure have been reported to be largely unaffected by climate variability (Stabeno, Kachel, et al. 2012; Sherr, Sherr, and Ross 2013), cold years in the eastern Bering Sea, such as during this study, favor the production of abundant large crustacean zooplankton and euphausiids (Hunt et al. 2011). Therefore, the export of fecal pellets produced by abundant *C. marshallae* and *T. raschii* may be an important mechanism controlling the vertical flux of POC from the photic zone in late spring and early summer during cold years.

Comparing the sinking loss rates of the pigments associated with zooplankton fecal pellets and diatoms with those for POC and TChl *a* provides insight into how these constituents influence particle flux from the surface ocean. It is assumed that phaeopigment fluxes are attributed to sinking zooplankton fecal pellets and fucoxanthin and bSi fluxes are associated with diatom export. Sinking loss rates for these exported constituents are estimated as the ratio of the flux determined at 50 m compared with the standing stock in the photic zone (Loss Rate = $\text{Flux}_{50\text{m}}$/Standing Stock; Thibault et al. 1999). At all trap locations, the loss of bSi, fucoxanthin, and Σphaeopigments from the photic zone represents a larger fraction of the standing stock than for either POC or TChl *a* (Table 7). Specifically, bSi, fucoxanthin, and Σphaeopigment loss rates range from 11% to 49% (excluding the single observation from HLY0902), 14% to 83%, and 5% to 100% per day, respectively. By comparison, loss rates of TChl *a* and POC are less than ∼7% d^{-1} (Table 7). Because bSi, fucoxanthin, and Σphaeopigment loss rates greatly exceed those for POC and TChl*a*, it follows that diatoms are preferentially transported to depth via zooplankton grazing and subsequent

Table 7. Photic zone stock of particulate organic carbon (POC; mmol m^{-2}) and biogenic silica (bSi; mmol m^{-2}), total chlorophyll *a* (TChl *a*; mg m^{-2}), phaeopigment sum (Σphaeopigments, phaeophytin *a*+ phaeophorbide *a*; mg m^{-2}), and fucoxanthin (mg m^{-2}) together with daily loss rates and fraction of total POC flux associated with TChl *a* (F Chl *a* [C]) and phaeopigments (F phaeo [C]). PAR, photosynthetically active radiation.

			Photic zone stock					Loss due to flux						
Cruise	Station	1% PAR m	POC mmol m^{-2}	bSi mmol m^{-2}	TChl *a* mg m^{-2}	ΣPhaeopigments mg m^{-2}	Fucoxanthin mg m^{-2}	POC % d^{-1}	bSi % d^{-1}	TChl *a* % d^{-1}	ΣPhaeopigments % d^{-1}	Fucoxanthin % d^{-1}	F Chl *a* (C) % of C Flux	F phaeo (C) % of C Flux
HLY0802	NP15	100	–	–	13.7	–	1.8	–	–	1.6	–	26.2	–	–
	ZZ15	26	–	–	28.2	6.5	8.1	–	–	11.2	99.7	21.3	–	–
HLY0902	BL2	38	–	–	557.4	12.5	200.2	–	–	1.4	16.3	36.9	49.6	14.9
	BL15	38	–	300.6	535.1	10.4	200.2	–	2.3	3.3	17.3	23.8	20.6	6.2
	BL15-1	38	–	–	535.1	10.4	200.2	–	–	3.1	25.9	19.9	39.1	11.7
	BL21	33	–	559.3	1,051.3	39.6	432.0	–	–	0.7	5.0	41.4	10.6	3.2
KN195-10	NP15	20	–	–	4.4	0.5	1.4	–	–	4.5	–	–	9.8	2.9
	MN19	23	917.3	–	17.3	–	2.7	–	–	–	–	–	–	–
TN249	MN19	75	3,641.6	127.8	905.8	109.2	395.1	1.2	26.8	0.5	9.0	41.8	94.5	28.3
	NZ11.5	60	385.0	124.3	20.8	4.1	6.5	5.3	14.3	2.5	24.5	29.7	20.4	6.1
	CN17	32	623.0	81.1	74.3	18.3	29.9	2.5	14.6	0.8	29.1	32.3	145.3	43.6
	MN19-2	40	1,496.5	72.8	47.0	7.1	19.1	1.1	11.7	1.4	25.1	31.0	47.0	14.1
TN250	CN17	23	255.4	23.3	18.0	1.9	4.2	31.7	48.9	6.5	55.6	14.3	5.4	1.6
	NP14	33	450.5	27.2	21.8	1.3	4.9	6.8	24.8	1.7	44.5	25.9	7.9	2.4
	P14-7	38	425.0	24.0	20.3	0.9	3.1	3.6	15.2	0.3	24.3	32.1	5.6	1.7
	MN19	46	501.0	48.1	16.9	1.0	5.7	3.4	10.5	1.2	37.8	83.6	9.5	2.9

production of fecal pellets. It must be noted that because the autotrophic community is actively growing, photic zone phaeopigment concentrations are low, relative to chlorophyll *a*, which leads to relatively large phaeopigment loss rates. However, the implication of the high loss rates is that almost all degraded chlorophyll *a* is being rapidly removed by the sinking of zooplankton fecal pellets.

The POC associated with TChl *a* and phaeopigment export can be estimated using generalized POC:TChl *a* and POC:phaeopigment ratios of 50:1 and 15:1 (Thibault et al. 1999). A POC:phaeopigment ratio of 15:1 assumes a 70% carbon assimilation efficiency by zooplankton (Thibault et al. 1999). POC fluxes associated with TChl *a* and phaeopigment export range from 5% to 100% and 2% to 44% of the total POC flux at 50 m, respectively (Table 7). The total carbon export by zooplankton is likely underestimated because respiration and excretion below the photic zone during daily vertical migration by mesozooplankton represents a significant component of the total C flux attributed to zooplankton (Hannides et al. 2009). In addition, ~20% of the POC associated with fecal pellets is likely released below the photic zone or below the deepest sediment trap in this study (Durbin et al. 1995). These results indicate that the export of zooplankton fecal pellets represents an important component of POC export along the shelf break in this region.

b. Elemental composition of phytoplankton and zooplankton-controlled export

As described previously, autotrophic biomass in the eastern Bering Sea during this study is composed predominantly of diatoms, and export of this algal group appears to be controlled by sinking zooplankton fecal pellets in spring and early summer. A quantitative understanding of the C:P and N:P ratios of phytoplankton in the photic zone and these elemental ratios in passively sinking particles can be used to make further inferences into the degree of zooplankton assimilation of these macronutrients, the efficiency of zooplankton-controlled particle export, and the potential stoichiometric ratios resulting from respiration and inorganic and organic excretion by zooplankton.

On average, phytoplankton in the photic zone of the eastern Bering Sea are rich in phosphorus relative to both carbon and nitrogen based on the Redfield C:N:P stoichiometric relationship of 106:16:1 (Fig. 7; Table 3). For this region in 2010, the average particulate C:P and N:P ratios in the upper water column were 87 ± 44 and 12 ± 5, respectively, both of which are less than the Redfield ratio. Collectively, 86% and 92% of all measurements from 2010 exhibit ratios lower than Redfield for C:P and N:P, respectively; note that C:P and N:P ratios of phytoplankton are plotted against absolute and relative fucoxanthin (i.e., fuco:TChl *a*) concentrations (Fig. 7). Although stoichiometric ratios of phytoplankton cannot be differentiated between spring and summer, the C:P and N:P ratios of suspended particles is invariant with the concentration of fucoxanthin or the fuco:TChl *a* ratio, suggesting that C:P and N:P do not vary with changing diatom biomass or autotrophic community composition (Fig. 7).

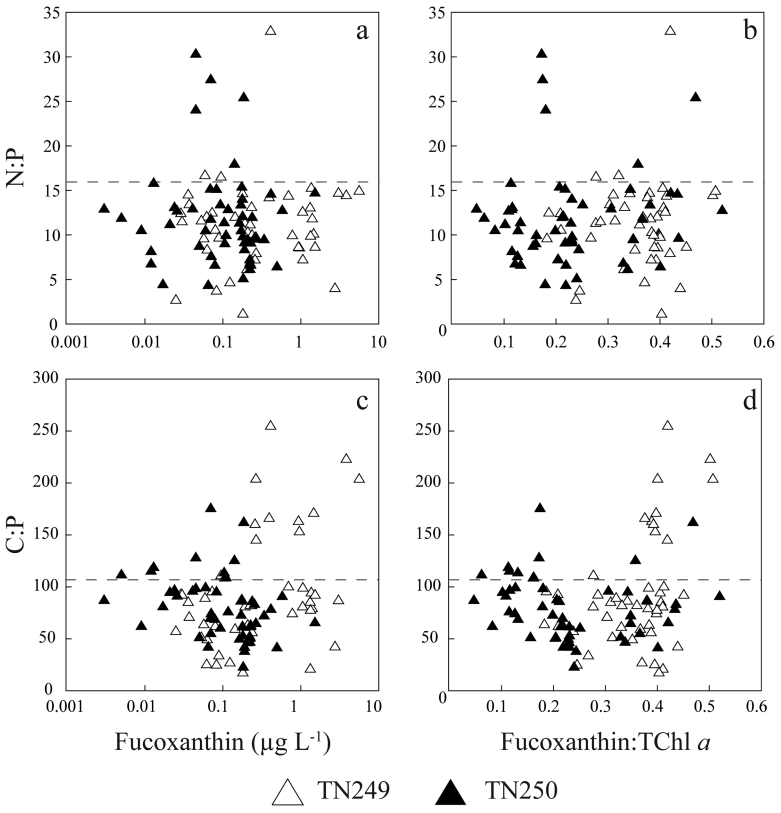

Figure 7. N:P (a and b) and C:P (c and d) of suspended particulate organic matter plotted against fucoxanthin concentration (μg L^{-1}; a and c) and the ratio of fucoxanthin to total chlorophyll *a* (TChl *a*; b and d). Reference lines of 16:1 and 106:1 are drawn for N:P and C:P, respectively, for comparison of the data.

There are a limited number of elevated N:P ratios at relatively low fucoxanthin concentrations (Fig. 7a). Each of these elevated N:P ratios are >20 and observed in different profiles collected during TN250. These few values are not consistent with other ratios from the same profiles and may not be representative of the water column at those locations. However, elevated C:P ratios are present at higher fucoxanthin concentrations and fuco:TChl *a* ratios (Fig. 7c and d). These high C:P ratios are found consistently at three stations (TN249; NZ4.5, HBR1, and 70M26), all of which are in region 4, near the ice edge, and have low surface-dissolved PO_4^{3-} concentrations (unpublished data). The relatively high biomass at these stations is supported by an autotrophic composition consisting of >90% diatoms and high concentrations of TChl *a* and bSi in a range similar to those measured at the bloom station (BL) in spring 2009. Thus, the diatom community at these stations may be a post-bloom population (Arrigo 2005).

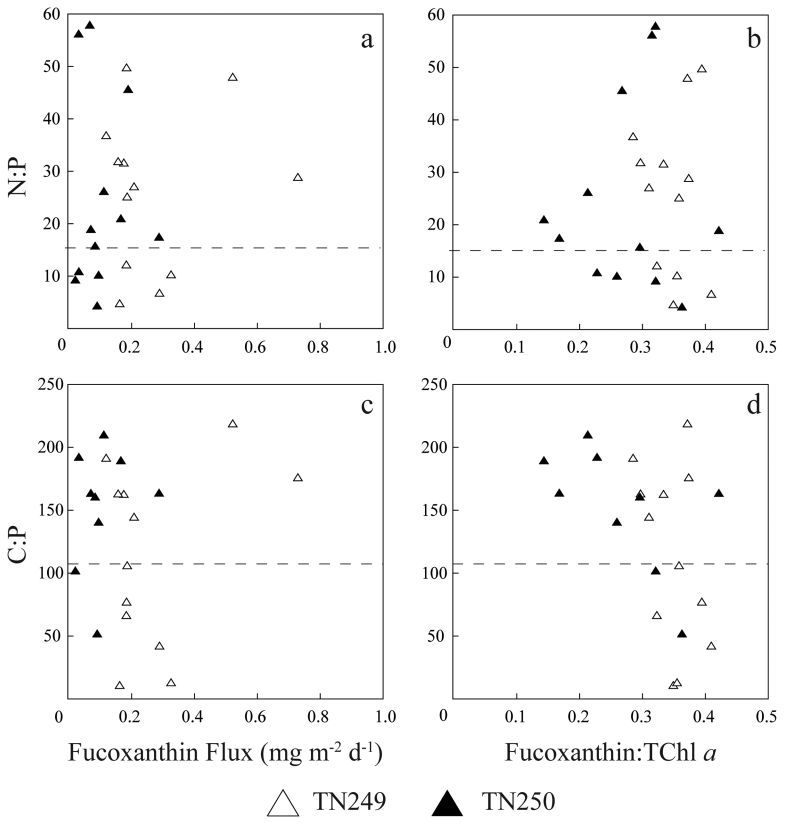

Figure 8. N:P (a and b) and C:P (c and d) of the vertical flux of particulate organic matter plotted against fucoxanthin flux (mg $m^{-2}d^{-1}$; a and c) and the flux ratio of fucoxanthin to total chlorophyll *a* (TChl*a*; b and d). Reference lines of 16:1 and 106:1 are drawn for N:P and C:P, respectively, for comparison of the data.

C:P and N:P ratios in sinking particles are substantially higher than those of water column–suspended particles, suggesting either carbon and nitrogen enrichment or phosphorus depletion of sinking zooplankton fecal pellets, relative to suspended particles. Sinking particles (40–100 m traps) exhibit average C:P ratios of 107 ± 71 (TN249) and 156 ± 67 (TN250) and average N:P ratios of 24 ± 14 (TN249) and 14 ± 8 (TN250) for spring and summer in 2010 (Table 4; Fig. 8). By comparison, fuco:TChl *a* ratios are similar in both phytoplankton and trap fluxes. For all six cruises, the average C:N of sinking particles was 7.3 ± 2.8 (Table 4). The average C:N ratio is consistent with the Redfield ratio of 6.6, which indicates that phosphorus depletion may be responsible for the high C:P and N:P values of sinking particles along the shelf break. An alternative explanation for the elevated C:P and N:P ratios is that the processes of inorganic and organic excretion by zooplankton may release relatively high proportions of phosphorus relative to carbon and nitrogen.

Weighted average C:P and N:P ratios of three subarctic copepods (*Calanus glacialis*, *Eucalanus* sp., and *Metridia pacifica*) and a euphausiid (*T. raschii*) are higher (C:P of 176 ± 52 and N:P of 35 ± 9; Lomas, M.W., Terpis, K.X., Campbell, R.G., and Ashjian, C.J., unpublished data) than the averages in the passively sinking particles these organisms produce. Although the standard deviations of these data are large, that the average C:P and N:P of these consumers is greater than the averages of both passively sinking particles and the phytoplankton in the water column suggests that the total excretion and respiration by zooplankton are likely enriched in phosphorus.

The C:P and N:P stoichiometry of the combined processes of respiration and inorganic/organic excretion by zooplankton may be important for both nutrient regeneration in the photic zone and export of carbon and nutrients to depth by vertical migration. These ratios may be estimated using a mass balance of the C:P and N:P of four pools: phytoplankton food source (P), zooplankton (Z), particle flux (F), and the combined processes of respiration and inorganic/organic excretion (A). The C:P and N:P ratios of respiration and excretion are calculated independently because carbon must be assimilated at a higher rate than nitrogen based on the high C:P of zooplankton in this region. Also, the C:P and N:P ratios of these pools need to be inversed (i.e., 1/C:P = P:C and 1/N:P = P:N) because A is calculated with respect to carbon and nitrogen, respectively. The mass balance equation for these nutrient pools is the following:

$$P = (Z \times ae) + (F \times f_1) + (A \times f_2), \tag{1}$$

where P, Z, F, and A are the P:C or P:N ratios of the four pools listed previously; ae is the carbon or nitrogen assimilation efficiency by zooplankton; and f_1 and f_2 are the fractions of carbon or nitrogen available (not assimilated) for particle export or for the combined processes of respiration and inorganic/organic excretion by zooplankton, respectively. Values of P, Z, and F are 87 ± 44, 175 ± 52, and 129 ± 72 for C:P, respectively, and 12 ± 5, 35 ± 9, and 21 ± 14 for N:P, respectively (Tables 3 and 4). With regard to estimating the C:P ratio for A, a range of zooplankton assimilation efficiencies (ae = 0.6 to 0.8; Hannides et al. 2009) and f_1 values (f_1 = 0.1 to 0.3) are used, while the relationship $1 - ae - f_1$ is substituted for f_2. For cases in which ae, f_1, and f_2 sum to 1, the average C:P ratio of A is 21 ± 9.7 (n = 89). The same approach is used for estimating the N:P ratio of A; however, a range of lower assimilation efficiencies are used because a larger fraction of the ingested nitrogen is likely excreted immediately (E. Durbin, personal communication). For the estimation of the N:P ratio, assimilation efficiencies range from 0.3 to 0.5, and f_1 ranges from 0.1 to 0.3. The ranges of ae and f_1 result in f_2 values that are generally larger than those used for the C:P ratio estimation, consistent with a larger fraction of excreted nitrogen. Solving equation (1) using these parameters yields an average N:P ratio of 6.3 ± 1.1 (n = 121) for A. Notwithstanding that the average C:P and N:P ratios calculated for A have large associated uncertainties that include large standard deviations of the P, Z, and F pools, and that the ae, f_1, and f_2 values are estimates from literature, these relatively low imputed ratios for A suggest that the processes of respiration and excretion are important for nutrient regeneration in the upper water column and export of carbon and nutrients to depth.

5. Summary and prospectus

During cold years in the eastern Bering Sea, the autotrophic community is dominated by diatoms in the spring and in the MIZ (Alexander and Niebauer 1981; Schandelmeier and Alexander 1981; Moran et al. 2012). Associated with a high percent composition of diatoms in spring is a greater frequency of elevated rates of net primary production and high levels of TChl *a* and POC in the photic zone. Despite a wide range in the magnitude of particle flux along the shelf break, the diatom algal class represents the majority of the exported TChl *a*. Because phaeophorbide *a* is present in large abundances in sinking particulate matter, often at levels much greater than TChl *a*, the vertical transfer of diatoms is likely mediated by enhanced zooplankton grazing of MIZ primary production and subsequent export of fecal pellets in late spring and early summer. Daily loss rates of fucoxanthin and phaeopigments from the photic zone exceed those for both TChl *a* and POC, supporting the notion that the sinking of zooplankton fecal pellets exerts an important control on particle and, specifically, diatom export from the surface waters along the shelf break. Further, zooplankton grazing may be an important process that returns nutrients, particularly phosphorus, to the dissolved inorganic pool in the upper water column.

This study provides new evidence of the relationship between the phytoplankton community and zooplankton-mediated export during cold years in the eastern Bering Sea, which will be necessary to interpret future observations in a changing Arctic climate. This region is predicted to warm in the coming decades (Overland and Wang 2007; Wang, Overland, and Stabeno 2012), resulting in a reduction in maximum sea-ice extent and earlier retreat in spring. As a consequence, the physical regime may restructure the spring autotrophic community to a population consisting of fewer large diatoms (principle prey source for large zooplankton) and increased abundance of smaller phytoplankton (Li et al. 2009), similar to summer conditions in this region. Total annual primary production may be greater in years characterized by early sea-ice retreat (Brown, van Dijken, and Arrigo 2011; Brown and Arrigo 2013); however, warm years are unfavorable for large zooplankton (Hunt et al. 2011). A reduction in large zooplankton may threaten the success of economically important animals (e.g., walleye pollock). Associated with this climate-driven shift of the autotrophic and zooplankton community may be a reduction in POC transfer to deeper waters and greater organic carbon retention within the water column. A further implication of a warming Bering Sea is the magnitude to which this subarctic shelf system sequesters carbon to the deep ocean (Baumann, Moran, Kelly, et al. 2013; Baumann, Moran, Lomas, et al. 2013), which may decrease in the future.

Acknowledgments. We thank the chief scientists, officers, and crew of the USCGC *Healy*, R/V *Knorr*, and R/V *Thomas G. Thompson* for their efforts. We also thank John Karavias of Walt Whitman High School (Queens, NY) and Jason Pavlich of Red Hook High School (Red Hook, NY) for their assistance as part of the ARMADA Project. We thank the hydrographic team from NOAA-Pacific Marine Environmental Laboratory, especially Sigrid A. Salo and Edward D. Cokelet, for providing hydrographic data and assisting in sample collection, accessible through the Earth Observing Laboratory data archive supported by NSF and NOAA. We thank Emily Goldman for assistance with the

CHEMTAX analysis. Finally, we thank Dr. Lee Cooper for his constructive comments that greatly improved this manuscript. This research was supported by awards ARC-0732680 and NPRB-B56 to SBM and ARC-0732359 to MWL.

APPENDIX TABLES

Table A1. Coordinate locations of all stations sampled for autotrophic pigments; particulate organic carbon, nitrogen, and phosphorus; and biogenic silica.

Cruise	Station ID	Latitude (° N)	Longitude (° W)	Cruise	Station ID	Latitude (° N)	Longitude (° W)
Region 1: spring				Region 1: summer			
HLY0802	SL12	62.19	175.13	KN195-10	MN3	59.86	168.90
HLY0802	SL6	61.96	171.22	KN195-10	SL6	62.20	171.89
HLY0902	MNSL4	61.78	176.80	TN250	ML3	61.97	170.78
HLY0902	SL9	62.09	173.28	TN250	BN3	62.67	173.38
HLY0902	SL1	61.70	167.75				
HLY0902	BN1	62.25	172.51				
HLY0902	SL12	62.19	175.15				
TN249	70M52	61.41	173.74				
TN249	SL12	62.19	175.15				
TN249	MN8	59.90	172.20				
Region 2: spring				Region 2: summer			
HLY0802	MN8.5	59.88	172.68	KN195-10	XB6	59.72	170.31
HLY0802	MN15	59.90	176.42	KN195-10	XB2-12	59.56	175.20
HLY0802	BS1	57.83	171.75	KN195-10	70M41	59.91	172.42
HLY0802	BS2	57.94	173.87	TN250	MN16	59.90	177.00
HLY0802	ZZ14	59.20	175.91	TN250	70M39	59.83	171.77
HLY0802	ZZ27	59.20	175.98				
HLY0902	MN4.5	59.94	169.99				
HLY0902	MN5	59.90	170.40				
HLY0902	MN13	59.87	175.21				
HLY0902	BL1	59.57	175.20				
HLY0902	BL4	59.54	175.03				
HLY0902	BL15	59.54	175.14				
HLY0902	BL20	59.54	175.14				
HLY0902	BL21	59.46	174.07				
HLY0902	70M42	60.00	172.73				
TN249	Z15	58.36	171.80				
TN249	IE1	59.33	175.61				

(Continued)

Table A1. (Continued)

Cruise	Station ID	Latitude (° N)	Longitude (° W)	Cruise	Station ID	Latitude (° N)	Longitude (° W)
Region 3: spring				Region 3: summer			
HLY0902	NP1	59.76	167.81	KN195-10	CN2	57.56	162.13
TN249	NP3	56.28	171.06	KN195-10	X3	58.78	166.72
				TN250	MN1	55.90	167.74
Region 4: spring				Region 4: summer			
HLY0802	NP7	57.92	169.19	KN195-10	NP7	57.90	169.24
HLY0902	NP6.5	58.04	169.23	KN195-10	XB16	57.16	172.94
HLY0902	NP9	57.45	169.78	KN195-10	70M25	58.05	169.65
HLY0902	NP11	56.98	170.28	TN250	UAP5	55.53	163.98
TN249	NP12	56.73	171.57	TN250	CNN4	57.35	167.04
TN249	NZ4.5	59.07	170.17	TN250	NP9	57.44	169.82
TN249	HBR1	56.93	167.32				
TN249	70M26	58.17	169.91				
TN249	70M29	58.62	170.28				
Region 5: spring				Region 5: summer			
TN249	NP14	56.28	171.05	KN195-10	UAP3	55.96	163.14
TN249	70M4	56.86	164.51	KN195-10	CN12	56.14	166.11
				KN195-10	CNN6	56.75	167.87
				TN250	CN8	56.71	164.51
				TN250	70M9	57.26	165.75
Region 6: spring				Region 6: summer			
HLY0902	MN19	59.90	178.90	KN195-10	SB7	57.28	173.84
TN249	MN19	59.90	178.91	KN195-10	X4	58.27	174.56
TN249	MN19	59.90	178.91	KN195-10	MN19	59.90	178.80
TN249	NZ11.5	58.21	174.25	TN250	TR4	59.90	178.88
TN249	MN19	59.90	178.91				
Region 7: spring				Region 7: summer			
HLY0802	NP15	56.26	171.13	KN195-10	CN20	55.03	169.22
TN249	CN17	55.43	169.06	KN195-10	NP15	56.05	171.30
				TN250	CN17	55.43	168.06
				TN250	TD2	56.25	171.11
				TN250	TR3	58.26	174.56

Table A2. Initial pigment:chlorophyll *a* matrix used for the CHEMTAX analysis together with final matrices for the water column and sediment trap analyses. Allox, alloxanthin; Chl *a*, chlorophyll *a*; Chl *b*, chlorophyll *b*; Diadinox, diadinoxanthin; Fuco, fucoxanthin; Neo, neoxanthin; 19′-But, 19′-butanoyloxyfucoxanthin; 19′-Hex, 19′-hexanoyloxyfucoxanthin Peri, peridinin; Prasinox, prasinoxanthin; Violax, violaxanthin; Zeax, zeaxanthin.

	Peri	19′-But	Fuco	19′-Hex	Neo	Violax	Diadinox	Allox	Prasinox	Zeax	Chl *b*	Chl *a*
Initial matrix												
Diatoms	0	0	0.377	0	0	0	0.121	0	0	0	0	0.503
Prymnesiophytes	0	0	0	0.547	0	0	0.063	0	0	0	0	0.391
Pelagophytes	0	0.311	0.207	0	0	0	0.147	0	0	0	0	0.334
Chlorophytes	0	0	0	0	0.028	0.021	0	0	0	0.043	0.199	0.709
Parasinophytes	0	0	0	0	0.045	0.045	0	0	0.146	0	0.360	0.405
Cryptophytes	0	0	0	0	0	0	0	0.123	0	0	0	0.877
Dinoflagellates	0.346	0	0	0	0	0	0	0	0	0	0	0.654
Cyanobacteria	0	0	0	0	0	0	0	0	0	0.248	0	0.752
Final matrix: water column												
Diatoms	0	0	0.287	0	0	0	0.021	0	0	0	0	0.692
Prymnesiophytes	0	0	0	0.287	0	0	0.001	0	0	0	0	0.712
Pelagophytes	0	0.269	0.221	0	0	0	0.195	0	0	0	0	0.315
Chlorophytes	0	0	0	0	0.024	0.017	0	0	0	0.010	0.383	0.566
Parasinophytes	0	0	0	0	0.077	0.085	0	0	0.302	0	0.080	0.457
Cryptophytes	0	0	0	0	0	0	0	0.238	0	0	0	0.762
Dinoflagellates	0.421	0	0	0	0	0	0	0	0	0	0	0.579
Cyanobacteria	0	0	0	0	0	0	0	0	0	0.567	0	0.433
Final matrix: sediment trap												
Diatoms	0	0	0.255	0	0	0	0.030	0	0	0	0	0.714
Prymnesiophytes	0	0	0	0.692	0	0	0.123	0	0	0	0	0.185
Pelagophytes	0	0.285	0.379	0	0	0	0.029	0	0	0	0	0.307
Chlorophytes	0	0	0	0	0.026	0.017	0	0	0	0.011	0.370	0.576
Parasinophytes	0	0	0	0	0.066	0.066	0	0	0.216	0	0.053	0.599
Cryptophytes	0	0	0	0	0	0	0	0.939	0	0	0	0.061
Dinoflagellates	0.346	0	0	0	0	0	0	0	0	0	0	0.654
Cyanobacteria	0	0	0	0	0	0	0	0	0	0.268	0	0.732

Table A3. Final matrices in the CHEMTAX analysis of the water column samples using fucoxanthin:chlorophyll *a* ratios of 0.75, 0.35, and 1.1. Allox, alloxanthin; Chl *a*, chlorophyll *a*; Chl *b*, chlorophyll *b*; Diadinox, diadinoxanthin; Fuco, fucoxanthin; Neo, neoxanthin; 19′-But, 19′-butanoyloxyfucoxanthin; 19′-Hex, 19′-hexanoyloxyfucoxanthin Peri, peridinin; Prasinox, prasinoxanthin; Violax, violaxanthin; Zeax, zeaxanthin.

	Peri	19′-But	Fuco	19′-Hex	Neo	Violax	Diadinox	Allox	Prasinox	Zeax	Chl *b*	Chl *a*
Fuco:chl *a*: 0.75												
Diatoms	0	0	0.287	0	0	0	0.021	0	0	0	0	0.692
Prymnesiophytes	0	0	0	0.287	0	0	0.001	0	0	0	0	0.712
Pelagophytes	0	0.269	0.221	0	0	0	0.195	0	0	0	0	0.315
Chlorophytes	0	0	0	0	0.024	0.017	0	0	0	0.010	0.383	0.566
Parasinophytes	0	0	0	0	0.077	0.085	0	0	0.302	0	0.080	0.457
Cryptophytes	0	0	0	0	0	0	0	0.238	0	0	0	0.762
Dinoflagellates	0.421	0	0	0	0	0	0	0	0	0	0	0.579
Cyanobacteria	0	0	0	0	0	0	0	0	0	0.567	0	0.433
Fuco:chl *a*: 0.35												
Diatoms	0	0	0.288	0	0	0	0.021	0	0	0	0	0.691
Prymnesiophytes	0	0	0	0.287	0	0	0.002	0	0	0	0	0.711
Pelagophytes	0	0.283	0.197	0	0	0	0.203	0	0	0	0	0.317
Chlorophytes	0	0	0	0	0.025	0.017	0	0	0	0.011	0.387	0.561
Parasinophytes	0	0	0	0	0.074	0.081	0	0	0.296	0	0.075	0.474
Cryptophytes	0	0	0	0	0	0	0	0.238	0	0	0	0.762
Dinoflagellates	0.422	0	0	0	0	0	0	0	0	0	0	0.578
Cyanobacteria	0	0	0	0	0	0	0	0	0	0.545	0	0.455
Fuco:chl *a*: 1.1												
Diatoms	0	0	0.287	0	0	0	0.021	0	0	0	0	0.6918
Prymnesiophytes	0	0	0	0.288	0	0	0.001	0	0	0	0	0.7113
Pelagophytes	0	0.272	0.219	0	0	0	0.196	0	0	0	0	0.3129
Chlorophytes	0	0	0	0	0.024	0.016	0	0	0	0.010	0.382	0.5675
Parasinophytes	0	0	0	0	0.079	0.088	0	0	0.311	0	0.078	0.4439
Cryptophytes	0	0	0	0	0	0	0	0.236	0	0	0	0.7638
Dinoflagellates	0.435	0	0	0	0	0	0	0	0	0	0	0.5650
Cyanobacteria	0	0	0	0	0	0	0	0	0	0.575	0	0.4252

Table A4. Regional averages of mixed-layer depth (MLD; m), depth of the photic zone (1% photosynthetically active radiation [PAR]; m), and percent ice at stations within each region (% ice cover) together with MLD averages of temperature (°C), salinity (%), density (σ_t, Density −1,000 kg m^{-3}), dissolved oxygen (DO; μmol kg^{-1}), and DO saturation from equilibrium (ΔDO saturation; μmol kg^{-1}).

Region	n	MLD m	1% PAR m	% Ice cover	Temperature °C	Salinity %	σ_t kg m^{-3}	DO μmol kg^{-1}	ΔDO saturation μmol kg^{-1}
Spring									
1	10	36 ± 20	29 ± 8	69 ± 48	−1.32 ± 1.12	32.06 ± 0.44	25.78 ± 0.40	338.85 ± 20.78	−30.02 ± 28.54
2	17	46 ± 19	23 ± 11	43 ± 41	−1.40 ± 0.48	31.99 ± 0.25	25.72 ± 0.21	373.50 ± 39.13	3.77 ± 43.07
3	2	33 ± 8	28 ± 7	49 ± 70	−0.70 ± 1.16	31.16 ± 0.37	25.02 ± 0.34	364.52 ± 16.30	−1.03 ± 26.03
4	9	40 ± 23	26 ± 10	38 ± 47	−1.05 ± 0.93	31.51 ± 0.45	25.32 ± 0.39	366.51 ± 27.46	−1.30 ± 33.15
5	2	38 ± 5	16 ± 0		1.14 ± 0.40	31.58 ± 0.02	25.28 ± 0.03	376.87 ± 3.77	29.85 ± 6.67
6	5	23 ± 20	22 ± 18	7 ± 17	−0.51 ± 1.42	32.32 ± 0.41	25.96 ± 0.38	384.42 ± 44.60	24.00 ± 49.42
7	2	43 ± 25	15	0	1.92 ± 1.38	32.44 ± 0.12	25.91 ± 0.18	329.74 ± 10.69	−8.40 ± 20.79
Summer									
1	4	26 ± 13	30 ± 9	0	3.43 ± 1.68	31.17 ± 0.40	24.83 ± 0.23	341.19 ± 26.21	12.06 ± 13.52
2	5	17 ± 7	29 ± 5	0	5.28 ± 0.80	31.61 ± 0.75	25.00 ± 0.57	326.15 ± 10.76	12.82 ± 12.71
3	3	25 ± 14	23 ± 9	0	3.52 ± 0.30	31.27 ± 0.23	24.93 ± 0.18	347.93 ± 33.30	20.29 ± 33.39
4	6	24 ± 6	29 ± 4	0	4.43 ± 1.20	31.54 ± 0.39	25.00 ± 0.25	340.51 ± 9.10	20.40 ± 3.45
5	5	19 ± 6	31 ± 8	0	5.06 ± 1.40	31.64 ± 0.12	25.03 ± 0.09	330.88 ± 12.01	15.80 ± 5.10
6	4	22 ± 5	32 ± 8	0	6.05 ± 0.57	32.75 ± 0.13	25.81 ± 0.15	321.90 ± 13.73	16.85 ± 11.85
7	5	29 ± 25	32 ± 5	0	5.79 ± 0.38	32.60 ± 0.14	25.69 ± 0.11	312.84 ± 7.33	5.69 ± 6.94

REFERENCES

Alexander, V., and H. J. Niebauer. 1981. Oceanography of the eastern Bering Sea ice-edge zone in Spring. Limnol. Oceanogr., *26*, 1111–1125.

Arrigo, K. R. 2005. Marine microorganisms and global nutrient cycles. Nature, *437*, 349–355.

Asper, V. L., and W. O. Smith Jr. 1999. Particle fluxes during austral spring and summer in the southern Ross Sea, Antarctica. J. Geophys. Res.: Oceans, *104*, 5345–5359.

Baumann, M. S., S. B. Moran, R. P. Kelly, M. W. Lomas, and D. H. Shull. 2013. ^{234}Th balance and implications for seasonal particle retention in the eastern Bering Sea. Deep Sea Res., Partt II, *94*, 7–21.

Baumann, M. S., S. B. Moran, M. W. Lomas, R. P. Kelly, and D. W. Bell. 2013. Seasonal decoupling of particulate organic carbon export and net primary production in relation to sea-ice at the shelf break of the eastern Bering Sea: Implications for off-shelf carbon export. J. Geophys. Res.: Oceans, *118*, 5504–5522.

Bianchi, T. S., C. Rolff, B. Widbom, and R. Elmgren. 2002. Phytoplankton pigments in Baltic Sea seston and sediments: Seasonal variability, fluxes, and transformations. Estuarine, Coastal Shelf Sci., *55*, 369–383.

Brown, Z. W., and K. R. Arrigo. 2013. Sea ice impacts on spring bloom dynamics and net primary production in the Eastern Bering Sea. J. Geophys. Res.: Oceans, *118*, 43–62. doi: 10.1029/2012JC008034

Brown, Z. W., G. L. van Dijken, and K. R. Arrigo. 2011. A reassessment of primary production and environmental change in the Bering Sea. J. Geophys. Res.: Oceans, *116*, C08014. doi: 10.1029/2010JC006766

Brzezinski, M. A., and D. M. Nelson. 1995. The annual silica cycle in the Sargasso Sea near Bermuda. Deep Sea Res., Part I, *42*, 1215–1237.

Cavalieri, D. J., T. Markus, and J. C. Comiso. 2014. AMSR-E/Aqua Daily L3 12.5 km Brightness Temperature, Sea Ice Concentration, & Snow Depth Polar Grids. Version 13. Boulder, CO: NASA Distributed Active Archive Center at the National Snow and Ice Data Center. doi: 10.5067/AMSR-E/AE_SI12.003

Cooper, L. W., M. A. Janout, K. E. Frey, R. Pirtle-Levy, M. L. Guarinello, J. M. Grebmeier, and J. R. Lovvorn. 2012. The relationship between sea ice break-up, water mass variation, chlorophyll biomass, and sedimentation in the northern Bering Sea. Deep Sea Res., Part II, *65–70*, 141–162.

Cooper, L. W., M. G. Sexson, J. M. Grebmeier, R. Gradinger, C. W. Mordy, and J. R. Lovvorn. 2013. Linkages between sea-ice coverage, pelagic–benthic coupling, and the distribution of spectacled eiders: Observations in March 2008, 2009 and 2010, northern Bering Sea. Deep Sea Res., Part II, *94*, 31–43.

Dunbar, R. B., A. R. Leventer, and D. A. Mucciarone. 1998. Water column sediment fluxes in the Ross Sea, Antarctica: Atmospheric and sea ice forcing. J. Geophys. Res.: Oceans, *103*, 30741–30759.

Durbin, E. G., R. G. Campbell, S. L. Gilman, and A. G. Durbin. 1995. Diel feeding behavior and ingestion rate in the copepod *Calanus finmarchicus* in the southern Gulf of Maine during late spring. Cont. Shelf Res., *15*, 539–570.

Fujiki, T., K. Matsumoto, M. C. Honda, H. Kawakami, and S. Watanabe. 2009. Phytoplankton composition in the subarctic North Pacific during autumn 2005. J. Plankton Res., *31*, 179–191.

Gleiber, M. R., D. K. Steinberg, and H. W. Ducklow. 2012. Time series of vertical flux of zooplankton fecal pellets on the continental shelf of the western Antarctic Peninsula. Mar. Ecol.: Prog. Ser., *471*, 23–36.

Grebmeier, J. M., L. W. Cooper, H. M. Feder, and B. I. Sirenko. 2006. Ecosystem dynamics of the Pacific-influenced northern Bering and Chukchi Seas in the Amerasian Arctic. Prog. Oceanogr., *71*, 331–361.

Grebmeier, J. M., J. E. Overland, S. E. Moore, E. V. Farley, E. C. Carmack, L. W. Cooper, K. E. Frey, J. H. Helle, F. A. McLaughlin, and S. L. McNutt. 2006. A major ecosystem shift in the northern Bering Sea. Science, *311*, 1461–1464.

Hannides, C. C. S., M. R. Landry, C. R. Benitez-Nelson, R. M. Styles, J. P. Montoya, and D. M. Karl. 2009. Export stoichiometry and migrant-mediated flux of phosphorus in the North Pacific Subtropical Gyre. Deep Sea Res., Part I, *56*, 73–88.

Heintz, R. A., E. C. Siddon, E. V. Farley Jr., and J. M. Napp. 2013. Correlation between recruitment and fall condition of age-0 pollock (*Theragra chalcogramma*) from the eastern Bering Sea under varying climate conditions. Deep Sea Res., Part II, *94*, 150–156.

Horner, R., and G. C. Schrader. 1982. Relative contributions of ice algae, phytoplankton, and benthic microalgae to primary production in nearshore regions of the Beaufort Sea. Arctic, *35*, 485–503.

Hunt, G. L., Jr., K. O. Coyle, L. B. Eisner, E. V. Farley, R. A. Heintz, F. Mueter, J. M. Napp, et al. 2011. Climate impacts on eastern Bering Sea foodwebs: A synthesis of new data and an assessment of the Oscillating Control Hypothesis. ICES J. Mar. Sci., *68*, 1230–1243.

Hunt, G. L., Jr., P. Stabeno, G. Walters, E. Sinclair, R. D. Brodeur, J. M. Napp, and N. A. Bond. 2002. Climate change and control of the southeastern Bering Sea pelagic ecosystem. Deep Sea Res., Part II, *49*, 5821–5853.

Juul-Pedersen, T., C. Michel, and M. Gosselin. 2010. Sinking export of particulate organic material from the euphotic zone in the eastern Beaufort Sea. Mar. Ecol.: Prog. Ser., *410*, 55–70.

Juul-Pedersen, T., T. G. Nielsen, C. Michel, E. F. Møller, P. Tiselius, P. Thor, M. Olesen, E. Selander, and S. Gooding. 2006. Sedimentation following the spring bloom in Disko Bay, West Greenland, with special emphasis on the role of copepods. Mar. Ecol.: Prog. Ser., *314*, 239–255.

Krause, J. W., D. M. Nelson, and M. W. Lomas. 2009. Biogeochemical responses to late-winter storms in the Sargasso Sea, II: Increased rates of biogenic silica production and export. Deep Sea Res., Part I, *56*, 861–874.

Li, W. K. W., F. A. McLaughlin, C. Lovejoy, and E. C. Carmack. 2009. Smallest algae thrive as the Arctic Ocean freshens. Science, *326*, 539.

Lomas, M. W., N. R. Bates, R. J. Johnson, A. H. Knap, D. K. Steinberg, and C. A. Carlson. 2013. Two decades and counting: 24-years of sustained open ocean biogeochemical measurements in the Sargasso Sea. Deep Sea Res., Part II, *93*, 16–32.

Lomas, M. W., A. L. Burke, D. A. Lomas, D. W. Bell, C. Shen, S. T. Dyhrman, and J. W. Ammerman. 2010. Sargasso Sea phosphorus biogeochemistry: An important role for dissolved organic phosphorus (DOP). Biogeosciences, *7*, 695–710.

Lomas, M. W., S. B. Moran, J. R. Casey, D. W. Bell, M. Tiahlo, J. Whitefield, R. P. Kelly, J. T. Mathis, and E. D. Cokelet. 2012. Spatial and seasonal variability of primary production on the Eastern Bering Sea shelf. Deep Sea Res., Part II, *65–70*, 126–140.

Lovvorn, J. R., L. W. Cooper, M. L. Brooks, C. C. De Ruyck, J. K. Bump, and J. M. Grebmeier. 2005. Organic matter pathways to zooplankton and benthos under pack ice in late winter and open water in late summer in the north-central Bering Sea. Mar. Ecol.: Prog. Ser., *291*, 135–150.

Mackey, M. D., D. J. Mackey, H. W. Higgins, and S. W. Wright. 1996. CHEMTAX - a program for estimating class abundances from chemical markers: Application to HPLC measurements of phytoplankton. Mar. Ecol.: Prog. Ser., *144*, 265–283.

Moran, S. B., M. W. Lomas, R. P. Kelly, R. Gradinger, K. Iken, and J. T. Mathis. 2012. Seasonal succession of net primary productivity, particulate organic carbon export, and autotrophic community composition in the eastern Bering Sea. Deep Sea Res., Part II, *65–70*, 84–97.

Napp, J. M., and G. L. Hunt Jr. 2001. Anomalous conditions in the south-eastern Bering Sea 1997: Linkages among climate, weather, ocean, and biology. Fish. Oceanogr., *10*, 61–68.

Niebauer, H. J., V. Alexander, and S. M. Henrichs. 1995. A time-series study of the spring bloom at the Bering Sea ice edge I. Physical processes, chlorophyll and nutrient chemistry. Cont. Shelf Res., *15*, 1859–1877.

Obayashi, Y., E. Tanoue, K. Suzuki, N. Handa, Y. Nojiri, and C. S. Wong. 2001. Spatial and temporal variabilities of phytoplankton community structure in the northern North Pacific as determined by phytoplankton pigments. Deep Sea Res., Part I, *48*, 439–469.

Overland, J. E., and M. Y. Wang. 2007. Future regional Arctic sea ice declines. Geophys. Res. Lett., *34*, L17705. doi: 10.1029/2007GL030308

Paasche, E. 1973. Silicon and the ecology of marine plankton diatoms. I. *Thalassiosira pseudonana* (*Cyclotella nana*) grown in a chemostat with silicate as limiting nutrient. Mar. Biol., *19*, 117–126.

Pike, S. M., and S. B. Moran. 1997. Use of Poretics® 0.7 μm pore size glass fiber filters for determination of particulate organic carbon and nitrogen in seawater and freshwater. Mar. Chem., *57*, 355–360.

Rutgers van der Loeff, M. M., J. Friedrich, and U. V. Bathmann. 1997. Carbon export during the Spring Bloom at the Antarctic Polar Front, determined with the natural tracer ^{234}Th. Deep Sea Res., Part II, *44*, 457–478.

Schandelmeier, L., and V. Alexander. 1981. An analysis of the influence of ice on spring phytoplankton population structure in the southeast Bering Sea. Limnol. Oceanogr., *26*, 935–943.

Sherr, E. B., B. F. Sherr, and C. Ross. 2013. Microzooplankton grazing impact in the Bering Sea during spring sea ice conditions. Deep Sea Res., Part II, *94*, 57–67.

Siddon, E. C., R. A. Heintz, and F. J. Mueter. 2013. Conceptual model of energy allocation in walleye pollock (*Theragra chalcogramma*) from age-0 to age-1 in the southeastern Bering Sea. Deep Sea Res., Part II, *94*, 140–149.

Solórzano, L., and J. H. Sharp. 1980. Determination of total dissolved phosphorus and particulate phosphorus in natural waters. Limnol. Oceanogr., *25*, 754–758.

Springer, A. M., C. P. McRoy, and M. V. Flint. 1996. The Bering Sea Green Belt: Shelf-edge processes and ecosystem production. Fish. Oceanogr., *5*, 205–223.

Stabeno, P., J. Napp, C. Mordy, and T. Whitledge. 2010. Factors influencing physical structure and lower trophic levels of the eastern Bering Sea shelf in 2005: Sea ice, tides and winds. Prog. Oceanogr., *85*, 180–196.

Stabeno, P. J., E. V. Farley Jr., N. B. Kachel, S. Moore, C. W. Mordy, J. M. Napp, J. E. Overland, A. I. Pinchuk, and M. F. Sigler. 2012. A comparison of the physics of the northern and southern shelves of the eastern Bering Sea and some implications for the ecosystem. Deep Sea Res., Part II, *65–70*, 14–30.

Stabeno, P. J., N. B. Kachel, S. E. Moore, J. M. Napp, M. F. Sigler, A. Yamaguchi, and A. N. Zerbini. 2012. Comparison of warm and cold years on the southeastern Bering Sea shelf and some implications for the ecosystem. Deep Sea Res., Part II, *65–70*, 31–45.

Strickland, J. D. H., and T. R. Parsons. 1968. A Practical Handbook of Seawater Analysis. Ottawa: Fisheries Research Board of Canada, 311 pp.

Suzuki, K., C. Minami, H. Liu, and T. Saino. 2002. Temporal and spatial patterns of chemotaxonomic algal pigments in the subarctic Pacific and the Bering Sea during the early summer of 1999. Deep Sea Res., Part II, *49*, 5685–5704.

Syvertsen, E. E. 1991. Ice algae in the Barents Sea: Types of assemblages, origin, fate and role in the ice-edge phytoplankton bloom. Polar Res., *10*, 277–288.

Thibault, D., S. Roy, C. S. Wong, and J. K. Bishop. 1999. The downward flux of biogenic material in the NE subarctic Pacific: Importance of algal sinking and mesozooplankton herbivory. Deep Sea Res., Part II, *46*, 2669–2697.

Tsukazaki, C., K.-I. Ishii, R. Saito, K. Matsuno, A. Yamaguchi, and I. Imai. 2013. Distribution of viable diatom resting stage cells in bottom sediments of the eastern Bering Sea shelf. Deep Sea Res., Part II, *94*, 22–30.

Van Heukelem, L., and C. S. Thomas. 2001. Computer-assisted high-performance liquid chromatography method development with applications to the isolation and analysis of phytoplankton pigments. J. Chromatogr. A, *910*, 31–49.

Wang, M., J. E. Overland, and P. Stabeno. 2012. Future climate of the Bering and Chukchi Seas projected by global climate models. Deep Sea Res., Part II, *65–70*, 46–57.

Wassmann, P., M. Reigstad, T. Haug, B. Rudels, M. L. Carroll, H. Hop, G. W. Gabrielsen, et al. 2006. Food webs and carbon flux in the Barents Sea. Prog. Oceanogr., *71*, 232–287.

Received: *16 January 2014*; revised: *22 November 2014*.